The Grotte du Bison Neandertals (Arcy-sur-Cure, France)

Juliette Henrion, Bruno Maureille, Cédric Beauval, Nicolas Vanderesse, Jean-Jacques Hublin, Maurice Hardy

Journal of Human Evolution 199 (2025) 103631

Contents lists available at ScienceDirect

Journal of Human Evolution

journal homepage: www.elsevier.com/locate/jhevol

The Grotte du Bison Neandertals (Arcy-sur-Cure, France)

Juliette Henrion [a, *], Bruno Maureille [a], Cédric Beauval [b], Nicolas Vanderesse [a], Jean-Jacques Hublin [c, d], Maurice Hardy [e]

[a] Univ. Bordeaux, CNRS, Ministry of Culture, PACEA, UMR 5199, F-33600, Pessac, France
[b] Archéosphère SARL, 11500, Quillan, France
[c] Paléoanthropologie, CIRB, Collège de France, Université PSL, CNRS, 75005 Paris, France
[d] Max Planck Institute for Evolutionary Anthropology, 04103 Leipzig, Germany
[e] Univ. Paris 1 Panthéon-Sorbonne, Univ. Paris Ouest Nanterre La Défense, MSH Mondes—CNRS—Ministère de la Culture, ArScAn, UMR 7041, 92000, Nanterre, France

ARTICLE INFO

Article history:
Received 14 July 2024
Accepted 29 November 2024
Available online 26 December 2024

Handling Editor: Dr A Taylor

Keywords:
Mousterian
Morphology
Teeth
Wear
Odontogenesis
Enamel–dentine junction

ABSTRACT

The Grotte du Bison, in Arcy-sur-Cure (Yonne, France), yielded a large assemblage of 49 Neandertal remains from late Mousterian layers, offering critical insights for the study of Middle to Upper Paleolithic populations of Western Europe. Previous studies described the external morphology of 13 isolated teeth and a partial maxilla. Building on this previous work, the current study provides further descriptions and analyses of the remains, including one postcranial fragment, six cranial fragments, two maxillary fragments, and 40 isolated teeth. The dental remains are examined for a more detailed assessment of the metric and nonmetric variability of their external and internal morphologies. We focus our description on preservation, health status, and age at death, and we assess the minimum number of individuals. The dental variability is also compared to that of Middle and Upper Pleistocene hominins. Our results indicate that the collection represents at least nine to 17 individuals, comprising mostly children and adolescents. Five to seven pairings are identified based on shared dental traits, developmental criteria, such as perikymata and pitted hypoplasia, wear patterns, and taphonomic alterations. This collection exhibits characteristic Neandertal features, including occasionally markedly expressed traits (e.g., I^1 and P^3 ridging and tubercular expressions), as well as a homogenous expression of accessory structures (particularly for the molars). The highest morphological variability is observed on maxillary premolar roots, which display different stages of root fusion, mesially placed hypercementosis, and pulp cavity extension. This collection also reflects the morphological and behavioral diversity observed in the other Arcy-sur-Cure caves.

1. Introduction

Neandertal populations exhibit considerable biological diversity from the Middle to Upper Pleistocene, classified into several chronobiological stages, including early pre-Neandertals, pre-Neandertals, early Neandertals, and 'classic'/Late Neandertals (Dean et al., 1998). Similar to their emergence, the timing and processes surrounding the disappearance of the Late Neandertals remain elusive and are further complicated by the plurality of these processes across Western Eurasia during the marine isotope stage (MIS) 3 (e.g., Hublin, 2009; Higham et al., 2014; Hajdinjak et al., 2018; Peyrégne et al., 2019; Devièse et al., 2021; Mafessoni et al., 2020; Fuchs et al., 2024; Slimak et al., 2024). Additionally, the increasing number of modern human fossil discoveries continues to push back their arrival in these regions by up to 15,000 years (Hublin et al., 2012, 2015; Slimak et al., 2022; Pederzani et al., 2024).

Understanding the biological diversity of Late Neandertals is therefore essential for reconstructing their microevolutionary history. The Arcy-sur-Cure caves, located at the crossroads of the northern European plains and the westernmost edge of Eurasia (France and Spain), are particularly significant in this regard. These caves house the largest collection of human remains attributed to Late Neandertals from this period. While much of the research has traditionally focused on the fossils from the well-known Grotte du Renne, due to its association with

* Corresponding author.
E-mail address: juliette.henrion@u-bordeaux.fr (J. Henrion).

https://doi.org/10.1016/j.jhevol.2024.103631

Châtelperronian material, the current study shifts focus to provide a detailed descriptive and comparative analysis of the Neandertal remains from the Grotte du Bison. Our work aims to provide new insights into the biological variability of Late Neandertals in this pivotal geographic region.

Located north of the Morvan massif (Bourgogne-Franche-Comté, France; Fig. 1a), the Cure Valley hosts vast karstic systems within coral and marly limestone. This geological landscape is mainly shaped by the erosive processes of the river, as well as the orogenesis of the Alps and weathering (Baffier and Girard, 1997; Roblin-Jouve et al., 2018). Extensive networks of galleries and numerous caves are found on the southern limit of Arcy-sur-Cure township (Yonne, Bourgogne-Franche-Comté, France; Fig. 1b and c). The earliest recorded visits of the prehistoric caves date back to the mid-17th century (including A. Badin in 1666, G-L.L. de Buffon in 1740–59, P.H. Vibraye in 1859, and A. Parat in 1897–98; in the Grotte des Fées, Grotte du Trilobite, Grotte du Cheval, and Grande Grotte; Leroi-Gourhan, 1951, Fig. 1c). Only brief surveys were conducted before A. Leroi-Gourhan's multidisciplinary scientific project (1946–1963). These first excavations focused on Upper to Middle Paleolithic occupation levels in six caves and a gallery: the Grotte du Lion, Grotte du Loup, Grotte du Bison, Grotte du Renne with the associated Schoepflin gallery, Grotte de l'Hyène, and Lagopède (Leroi-Gourhan, 1952, Fig. 1c).

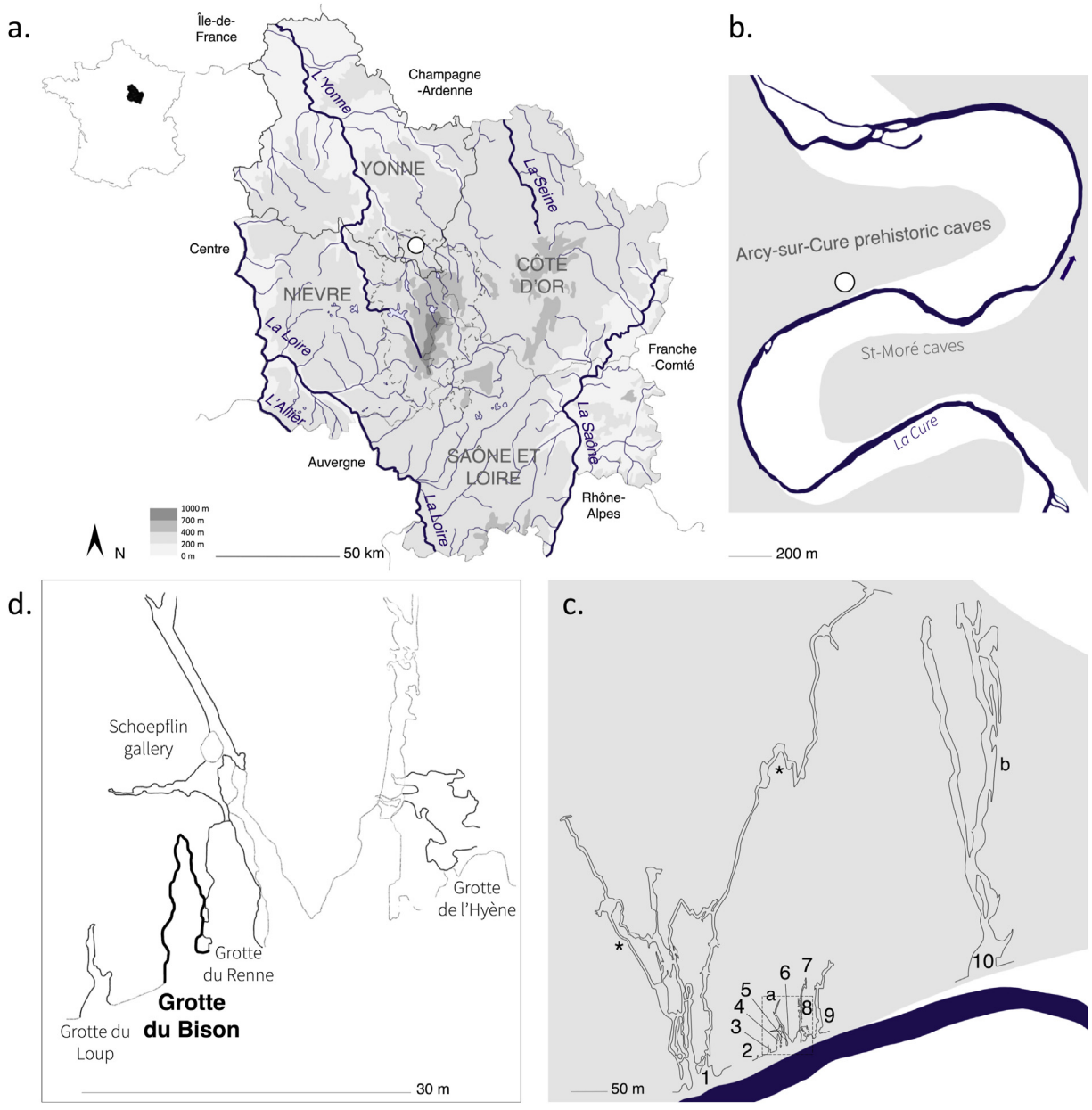

Figure 1. Location of Arcy sur cure in (a) Bourgogne-Franche-Comté (France); (b) with the karstic systems in the Cure meander; (c) where the Arcy-sur-Cure prehistoric caves are located (1. the Grotte des Fées; 2. Grotte du Lion; 3. Grotte du Loup; 4. Grotte du Bison; 5. Grotte du Renne and a. the Scheopflin gallery; 6. the Grotte de l'Ours; 7. the Grotte du Trilobite; 8. the Grotte de l'Hyène; 9. the Grotte du Cheval; 10. the Grande Grotte; and * undergroud rivers); (d) with the Grotte du Bison and the other caves holding Middle to Upper Pleistocene human remains (Adapted from Baffier and Girard, 1997; Tillier et al., 2013a).

Numerous Middle to Upper Pleistocene human fossils were discovered in five locations (i.e., Girard et al., 1990; Leroi-Gourhan, 1951, 1958, Fig. 1d). Only the Grotte du Renne held human remains in association with Upper Paleolithic material, with a few modern human remains ($n = 2$, in the Aurignacian layer VII, and $n = 1$ in the Chatelperronian layer X; Leroi-Gourhan, 1958; Maureille and Hublin, 2019; Gicqueau et al., 2023), and a substantial number of Neandertal remains uniquely associated with a rich Châtelperronian assemblage ($n = 68$ in layers X to VIII; Leroi-Gourhan, 1958, Hublin et al., 1996; Bailey and Hublin, 2006; Welker et al., 2016; Maureille and Hublin, 2019; Gravina et al., 2022; Henrion et al., 2023). The rest of the fossil collection consists of Neandertal remains strictly discovered within Mousterian units: 6 in the Grotte du Renne (layers XI and XIV; Maureille and Hublin, 2019); 5 in the Scheopflin gallery (layers IV2, IV5, and IV7; Maureille and Hublin, 2019; and ongoing project); 49 in the Grotte du Bison (layers G, I, and J; David et al., 2009; Tillier et al., 2013a, 2013b; and this current study); 18 in the Grotte de l'Hyène (layers IVa and IVb1, IVb3, IVb5, and IVb6; Leroi-Gourhan, 1958; and ongoing project); and 1 the of the Grotte du Loup (layer III; Leroi-Gourhan, 1958).

The Grotte du Bison collection is mostly unpublished, with 14 remains studied by David et al. (2009) and Tillier et al. (2013a, 2013b; cf. Table 1), yet the cave holds the second largest number of human fossils among the Arcy-sur-Cure sites, after its twin cavity the Grotte du Renne. We begin by describing the cranial and postcranial elements and then focus on the dental remains, including maxillary fragments and isolated teeth, representing more than 80% of the human fossil collection. We describe the preservation and the health status of the remains together with their external and internal morphology. Building upon classical anthropological analyses, our study delves into key nonmetric traits observable on the occlusal enamel surface (OES) and the corresponding enamel–dentine junction (EDJ). Moreover, we identify individual pairings through unique odontogenetic patterns, developmental features, and defects, in addition to morphological similarities and shared wear facets.

1.1. Fieldwork history of the Grotte du Bison

In 1958, during A. Leroi-Gourhan's fieldwork in Arcy-sur-Cure, P. Poulain discovered the Grotte du Bison from its concomitant wall with the Grotte du Renne (Fig. 2b). The following year, he conducted an initial survey in the front end of the cave (in Q–R7; Fig. 2b). R. Kapps and F. Hours then led the investigations in the cave with a couple of surveys in the entry area and a northeast section of the cave (a 2-m^2 survey in T–U14; Fig. 2b), in 1959 and from 1961 to 1963. By the end of A. Leroi-Gourhan's fieldwork (1963), the lowest Mousterian layer was reached in the latter survey, and two human teeth were uncovered (cf. Table 1).

The Grotte du Bison was the only cave in Arcy-sur-Cure to undergo further investigation following A. Leroi-Gourhan's fieldwork. From 1995 to 2010, the excavations resumed with new fieldwork directed by F. David, beginning with the clearing of the cave's talus and the 'Poulain survey'. Once the bedrock had been reached throughout the survey, the excavation area was expanded north, and a 3-m-thick sterile infilling was removed from the entry to the ancient gallery (David et al., 2006, Fig. 2b). Progressing from west to east, excavations reached layer J in 2008 (Fig. 2a). By 2011, 15 new human remains were discovered, with 10 teeth and 5 skeletal fragments mostly in layer I (cf. Tables 1 and 2). One of the authors (M.H.) then assumed directorship of the fieldwork (2012), clearing the remaining karstic blocs from layer I (from the collapsed roof and west wall of the cave) and reaching layer J throughout the cavity. The excavations concluded in 2019, and the following year, B.M., C.B., M.H., and P-J. Dodat conducted a thorough investigation of the entire faunal collection, resulting in the rediscovery of 15 new human pieces, including nine isolated teeth and five cranial fragments.

1.2. Topography, stratigraphy, and dating

During the excavations, three main areas were delineated based on the cave topography (Roblin-Jouve et al., 2018): the south-facing 'entry' ($\approx$20 m^2), the central 'parvis' ($\approx$50 m^2), and a narrowing 'gallery' with a preserved ceiling ($\approx$10 m^2, with a ceiling height of $\approx$0.60 m; Fig. 2b).

Two primary sedimentological processes contributed to the cave infilling (Girard et al., 1990; David et al., 2006; Roblin-Jouve et al., 2018): 1) clayey and sandy alluvial deposits from the Cure River dominate the base of the stratigraphy and 2) nearly constant karstic rockfall occurs from the earliest occupation layers to the upper layers, with persistent desquamation of the limestone and sporadic gelifraction events.

Eleven lithostratigraphic units are identified in the cave, labeled alphabetically from A at the top to K at the base (Fig. 2a). Above the bedrock, layers K and J are endokarstic layers. Layer K is archeologically sterile and delivers few faunal remains. Layer J marks the earliest human occupation(s) in the cave, with a Levallois Mousterian industry dominated by Charentian scrapers. Layer I is also a sandy alluvial unit characterized by Levallois Charentian Mousterian material but includes numerous large karstic blocks from cave walls and ceiling. Layers H and G include, respectively, karstic blocks and gelifraction clasts, with denticulate Mousterian material. Layers F and E are filled with rockfalls from the cave roof and walls, along with gelifraction blocks. Large limestone slabs separate these two layers; however, refitted lithics are found. Containing a Charentian Mousterian industry (richer in layer F), they represent the last Middle Paleolithic deposits. Layer D still contains limestone clasts embedded in clayey silts. Significant ceiling breakage events are evident at the top of these units, marking the transition of the cave into a rockshelter during the Châtelperronian occupations, at the base of layer D. Ultimately, the destruction of the porch defines the upper limit of this layer. Layers C and B correspond to the natural collapse of the remaining cave, whereas layer A represents modern infilling and the soil of the plateau.

Absolute dating was done on faunal remains and sediments from the archaeological layers using a set of alternative techniques (radiocarbon, electron spin resonance [ESR], and Uranium/Thorium [U/Th]). Part of the radiocarbon results have been published (David et al., 2006; Roblin-Jouve et al., 2009) and recently reassessed by M.H. alongside ESR and U/Th testing. The top of layer B yielded a radiocarbon date of 24140 $\pm$ 310 cal BP, and layer C yielded a date of 27006 $\pm$ 468 cal BP (Lyon 8825; David et al., 2006). Layer D is dated to 37195 $\pm$ 1323 cal BP (OxA 8091/Lyon 742) or between 31548 $\pm$ 330 and 37008 $\pm$ 1447 cal BP (Beta, 180086). Layers E and F range from 40887 $\pm$ 1167 cal BP (OxA10017, Ly1294) to 42121 $\pm$ 1206 cal BP (GrA20477, Ly1915). Layer I is dated from 45249 $\pm$ 1920 cal BP (Erl-16192) to 48323 $\pm$ 2811 cal BP (Erl-1692), with a 95.4% probability. The Layer J ESR calibrated date is 50837 $\pm$ 2376 cal BP.

Based on the technocultural attributions of the archaeological material and fauna assemblage, the human occupations likely span from MIS 2 to MIS 3, with Neandertal presence in the cave during early MIS 3 (Girard et al., 1990; David et al., 2006; Roblin-Jouve et al., 2018).

Table 1
Dental collection from the 'Grotte du Bison', including the specimen number, fieldwork label (indicating site 'A' for Arcy-sur-Cure followed by the year of discovery, cave 'B' for 'Grotte du Bison', the layer, location, and sometimes a specimen number, according to the discovery), archaeological layer (by stratigraphic unit), identification of the remains, occlusal wear stage, age estimation, and references for the published remains.

Specimen ID[a]	MNP label	Fieldwork label	Archaeological layer	Tooth class	Occlusal wear (Smith, 1984)	Occlusal wear (Molnar, 1871)[b]	Age class	Age estimation (years)	References
1	MNP 2013-6-1-1	A 1963 B J T14	J	LdP^4 germ	1	1; 1; 1	Infancy	1.5–2.5	Tillier et al. (2013a)
2	MNP 2013-6-1-2	A1963 B J2 U14 2931	J	LM^2	4	4; 2–4; 2	Young adult	20–25	Tillier et al. (2013a)
3		A2000 B G R8	G	RdC_1	4	4; 6; 3	Late childhood	7.5–10.5	
4		A2007 B I Q9 100	I	LP_3	(4)	(4; 3; 2)	Middle-aged adult	Middle-aged adult	
5		A2008 B I3 P8 63	I	LM^3	(4)	(4; 2; 3)	Middle-aged adult	Middle-aged adult	David et al. (2009); Tillier et al. (2013a)
6		A2008 B I3 P8 31	I	LM^1 germ	1	1; 1; 1	Early childhood	2.5–3.5	David et al. (2009); Tillier et al. (2013a)
7		A2008 B I3 Q8 121	I	RdI^1	2	2; 6; 2	Infancy	1.5–2.5	David et al. (2009); Tillier et al. (2013a)
8		A2008 G I3 R11	I	RC_1	4	4; 4; 3	Young adult	Young adult	
9		A2009 B I R10 7	I	RP_3	3	3; 4; 2	Young adult	Young adult	
10		A2010 B I P8	I	LM_1 germ	1	1; 1; 1	Early childhood	2.5–3.5	Tillier et al. (2013a)
11		A2010 B S15 1	J	LI^1	2	2; 2; 2	Preadolescence	8.5–11.5	Tillier et al. (2013a)
12		A2010 B J P7 76	J	LM_3	3	2; 3; 3	Young adult	Young adult	Tillier et al. (2013a)
13		A2011 B I P8 101	I	$RM^{2/3}$ germ	1	1; 1; 1	Preadolescence	9.5–11.5	Tillier et al. (2013a)
14		A2011 B I P7 48	I	RM^1	(2)	(2; 2; 2)	Postadolescence	16.5–20	Tillier et al. (2013a)
15		A2011 B I O11 192	I	LdC^1	4	5; 2; 2	Preadolescence	8.5–10.5	Tillier et al. (2013a)
17		A2011 J P12 98	J	LC^1	4	5; 2; 3	Middle-aged adult	Middle-aged adult	
19		A2012 B I Q5 1	I	RdP_4	(5)	(5; 3; 2)	Late childhood	6.5–8.5	Tillier et al. (2013b)
20		A2012 B I S6 2	I	RdP_4	1	1; 1; 1	Infancy	1.5–2.5	Tillier et al. (2013b)
21		A2013 B J R9 1	J	RP_4	2	2; 3; 2	Full adolescence	12.5–13.5	
22		A2013 B J R9 2	J	$LM_{2/1}$	2	2; 3; 2	Postadolescence	16.5–20.5	
23		A2014 B J T12 35	J	RC_1	2	2; 3; 6	Preadolescence	11.5–12.5	
24		A2014 B J P6 1	J	LP_3 germ	1	1; 1; 1	Late childhood	5.5–6.5	
25		A2014 B J Q4 1	J	RP_4	4	4; 6; 2	Middle-aged to elder adult	Middle-aged to elder adult	
26		A2014 B J S10	J	LP_3	2	3; 3; 2	Full adolescence	ca. 12.5	
27		A2014 B J R12 27	J	$RM_{2/3}$	1	1; 1; 1	Full adolescence	10.5–11.5	
28		A2015 B J O9 1	J	$RM^{2/3}$	1	1; 1; 1	Full adolescence	11.5–12.5	
29		A2015 B J R12	J	RM^1 germ	1	1; 1; 1	Early childhood	ca. 3.5	
30		A2015 B J O11	J	LP^4	5	6; 4; 4	Middle-aged adult	Middle-aged adult	
32		A2017 B J2 P11 60	J	$LM^{2/3}$	1	1; 1; 1	Full adolescence	11.5–12.5	
33		A2017 B J S8 1	J	RP^3	2	2; 4; 2	Full adolescence	12.5–14.5	
34		A2017 B J P4/Q4 11	J	RM^3 germ	1	1; 1; 1	Full adolescence	14.5–15.5	
35		A2017 B J P12	J	RdP^4	(5)	(5; 6; 2)	Preadolescence	9.5–11.5	
37		A2019 B J2 P11	J	RM^1 germ	1	1; 1; 1	Full adolescence	ca. 3.5	
38		A2019 B J2 P8 30	J	RP^4	2	2; 1; 2	Full adolescence	ca. 13.5	
39		A2019 B J2 Q9 1	J	Maxilla (LP^3)	3	3; 4; 2	Young adult	Young adult	
				Maxilla (LP^4)	NA	NA			
40		A2019 B J2 P10 82	J	RM_2	2	2; 1; 2	Full adolescence	11.5–16.5	
41		A2019 B Q11 1		LM_2	3	2; 4; 3	Young adult	20–25	
42		A2019 B J2 S6 25	J	LM_1 germ	1	1; 1; 1	Early childhood	ca. 2.5	
43		A2019 B J2 O10 22a	J	LM_2	2	2; 3; 2	Full adolescence	11.5–16.5	
44		A2019 B J2 O10 22b	J	LM_3	1	1; 1; 1	Full adolescence	ca. 14.5	
45		A2019 B J2 Q10 65	J	LI^1	3	3; 2; 2	Preadolescence	8.5–11.5	
46		A2008 B I3 P11 8	I	Maxilla (RC^1)	4	4; 2; 3	Young adult	Young adult	David et al. (2009); Tillier et al. (2013a)
				Maxilla (RP^3)	4	4; 2; 3			
				Maxilla (RP^4)	4	4; 2; 4			
				Maxilla (RM^1)	5	5; 2; 2			
				Maxilla (RM^2)	4	4; 2; 3			
				Maxilla (RM^3)	3	4; 2; 3			

Abbreviations: ID = identification number of the specimen, in our study; MNP = Musée National de Préhistoire; L = left; R = right; NA = not acquired.
[a] Specimen ID numbers follow the order of discovery.
[b] The first number = occlusal attrition; the second = orientation of wear; the third number = surface general topography. Wear stages in parentheses indicate acidic, biochemical, and/or taphonomic alteration hindering the reading of the occlusal wear.

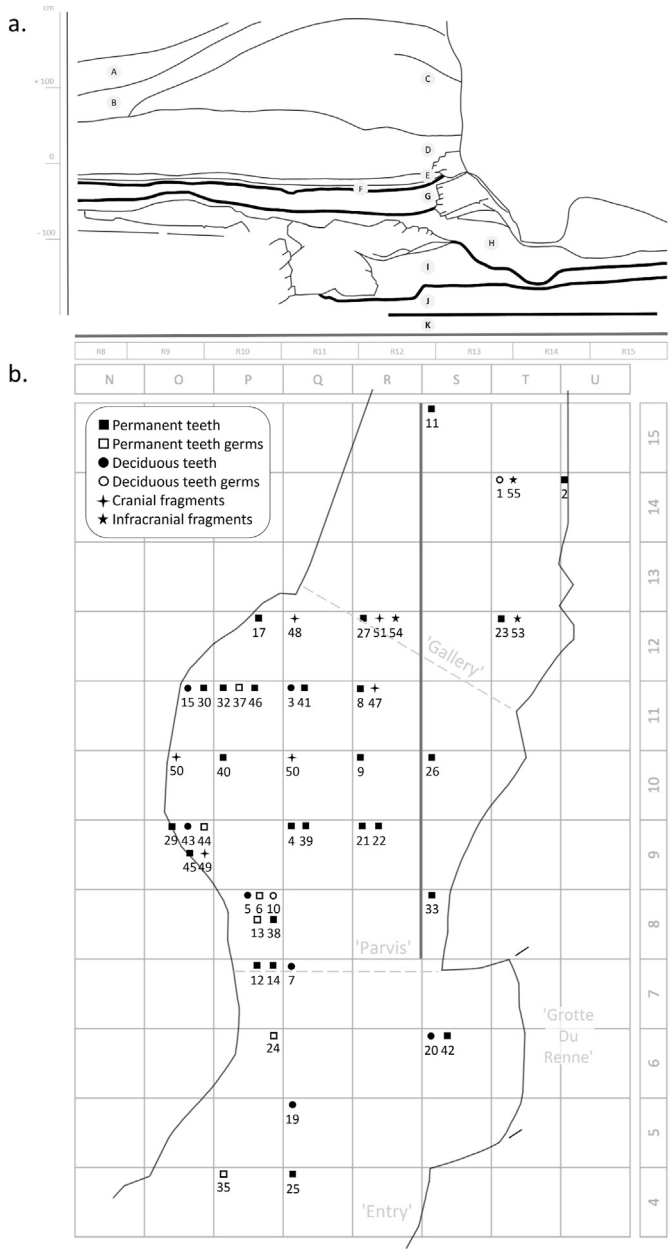

Figure 2. (a) Sagittal section (north-left and south-right) of the Grotte du Bison stratigraphy, with the layer containing the Neandertal fossils highlighted in bold and (b) the human remains distribution within the cave (identified by their specimen number—cf. Table 1—in the top left corner of their respective excavation square; modified from M.H. fieldwork reports).

1.3. Neandertal occupation and taphonomic evidence

Human activity is concentrated in the 'entry' and 'parvis' of the cave, spanning from the Mousterian sequence with layers J–E to the Châtelperronian layer D (Fig. 2a; David et al., 2006; Roblin-Jouve et al., 2018). Among those layers, the densest in archaeological materials are layers G and H, and evidence of fire is identified in layers E and F.

Within the Mousterian sequence, the carnivore occupations are intertwined with the human occupations, with *Ursus spelaeus* in layers H to D, where Neandertals accumulated reindeer, horses, and bison. Meanwhile, *Crocuta crocuta spelaea* occupations are identified in the layer I, where Neandertals accumulated *Equus* sp., *Cervus elaphus*, and *Bos priscus* (David et al., 2006; Tillier et al., 2013a).

As previously mentioned, all human remains are associated with Mousterian layers J and I, comprising 39 isolated teeth, two maxilla fragments, six cranial fragments, and at least one postcranial fragment. Additionally, one deciduous tooth was discovered within layer G.

A total of 13 isolated teeth and one maxilla fragment had been previously documented (Table 1) and identified as Neandertal (David et al., 2009; Tillier et al., 2013a, 2013b). Carnivore interactions with the hominin collection were highlighted through observations such as tooth marks on the infraorbital surface of a maxilla (David et al., 2009) and the discovery of two partially digested teeth (right M^3 and left dP_4; Tillier et al., 2013a, 2013b). Preliminary descriptions of nine isolated teeth were provided by A.M. Tillier in official field reports for the French Ministry of Culture (cataloged in the Bourgogne-Franche-Comté Archaeological Services library). However, the subsequent excavations did not involve comprehensive studies of the newly discovered human remains.

2. Material and methods

2.1. The human remains collection of the Grotte du Bison

The teeth (#1 and #2 in Table 1) discovered during A. Leroi-Gourhan excavations are currently preserved at the Musée National de Préhistoire (Eyzies-de-Tayac-Sireuil, France). The collection related to fieldwork conducted by F. David and M.H. is temporarily housed at the PACEA laboratory (University of Bordeaux, France) and is administered by the archaeological services of Bourgogne-Franche-Comté ('Service Régional d'Archéologie').

In the collection, one isolated tooth is from layer G, layer I includes 13 teeth, one fragmented hemimaxilla, and six cranial fragments, and layer J contains 26 teeth, one maxilla fragment, and one fibula diaphysis (Tables 1 and 2). In addition to the cranial fragments and fibula (Table 2), two postcranial fragments could be considered human (a rib and a long bone fragment) and are described in Supplementary Online Material (SOM) Figure S1.

The dental metric comparative dataset includes published data and unpublished measurements from the PACEA scientific members' database: 335 Neandertal, 207 early Neandertal, 108 pre-Neandertal, and 582 Upper Pleistocene modern human permanent teeth (SOM Table S1a), and 45 Neandertal, 12 early Neandertals, two pre-Neandertal, and 65 Upper Pleistocene modern human deciduous teeth (SOM Table S1b); geochronological group distinctions are based on Dean et al. (1998), Hublin (2009), and Peyrègne et al. (2019). Additionally, we include measurements of published and unpublished Neandertal teeth from Arcy-sur-Cure (permanent: $n = 16$; deciduous: $n = 3$; Bailey, 2006; Henrion et al., 2023). Holocene modern humans from Spitalfields and Poundbury in the UK, and Coxyde in Belgium, are added to the comparative fossil groups ($n = 496$; Maureille, 2001).

2.2. Digital data acquisition

The two teeth from the A. Leroi-Gourhan excavations were scanned in 2016 using micro-computed tomography (μCT) at the Max Planck Institute (MPI; Leipzig), with an isometric size of 16 μm (100 kV, 62 μA, using 1-mm aluminum filter, exposure time = 991 milliseconds [ms]). From 2019 to 2023, the remains from fieldwork conducted by F. David and M.H. were scanned at PLACAMAT (University of Bordeaux and CNRS, France, by N.V.) with

different scanning parameters. The isolated teeth and the #39 maxilla fragment were scanned with an isometric voxel size of 25 μm (100 kV, 300 μA, 0.1-mm copper filter, exposure time = 500 ms). Teeth #43 and #44, held within a concretion block, were scanned with an isometric voxel size of 31 μm (110 kV, 320 μA, 0.1-mm copper filter, exposure time = 500 ms). The fragmented hemimaxilla #46 was scanned at an isometric voxel size of 34 μm (120 kV, 200 μA, 0.1-mm copper filter, exposure time = 500 ms).

The acquired μCT scans were semiautomatically segmented using Avizo v. 8.1 (Visualization Sciences Group Inc., Berlin) to render the EDJ and pulp cavity morphology. The watershed tool was used to isolate the different materials (enamel, dentine, pulp cavity, bone, calculus, and sediments), and manual editing was needed due to the similar densities of the materials, namely the similar gray levels in the scans. Some EDJ reconstructions were interpolated from their negative surface on the enamel cap (#40, #42, and #43) due to the lack of dentine preservation. Furthermore, odontological observations for specimen pairing were conducted using VG StudioMax v. 3.5.0 (Volume Graphics GmbH, Heidelberg), with another segmentation needed to render a high-resolution three-dimensional surface (Le Cabec et al., 2015).

2.3. Morphological descriptions

The bone analyses focused on identification of taphonomic alterations, determination of maturation status, and morphological descriptions to identify the fragments and characterize their Neandertal-like features. The cranial and postcranial remains were analyzed following Gray et al. (2021) and White and Folkens (2005), with Mays (2016) and Byers (2002) for bone maturation references. The largest orthogonal dimensions of the remains were measured using 150-mm Mitutoyo digital calipers (0.01-mm accuracy) and the means used for metric comparisons.

The class-specific descriptions of each tooth encompass a concise overview of the preservation, health, and wear status (following both Smith, 1984; Molnar, 1971, Table 1), age-at-death determination, and the OES and EDJ morphologies. All the anatomical views of the dental remains and their associated EDJ surfaces are provided in SOM Figure S2.

Age at death for fossil individuals was determined through assessment of dental development, dental eruption, interproximal wear facets, and occlusal wear patterns (Moorrees et al., 1963; Brothwell, 1989; Miles, 2001; Liversidge and Molleson, 2004; AlQahtani et al., 2010, 2014; Shackelford et al., 2012). Precise age estimations in months or years, possible through dental development and eruption schedules, were conducted using a modern reference (e.g., AlQahtani et al., 2010, 2014), acknowledging potential biases introduced by this method. However, variability in rate of growth and, therefore, unknown differences in dental development across fossil hominin taxa, particularly between Neandertals and modern humans, pose challenges to accurate age estimation (Dean et al., 2001; Ramirez Rozzi and Bermudez de Castro, 2004; Macchiarelli et al., 2006; Smith et al., 2007, 2010). Thus, maturation standards were also used to categorize age at death, adopting broader classes such as infancy, childhood, adolescence, and adulthood (Sempé, 1978; Roksandic and Armstrong, 2011).

The morphology of the OES and EDJ is described following Scott and Irish (2017), Skinner et al. (2008), Skinner and Gunz (2010), and Chapple and Skinner (2023). The morphological nomenclature used is summarized in the SOM Figure S3, with the following abbreviations used for the main and accessory cusps: protocone/id (Pro); paracone/id (Pa), metacone/id (Met), entoconid (Ent), hypocone/id (Hyp), hypoconule/id (C5), entoconulid (C6), and metaconule/id (C7; Kanazawa et al., 1990; Turner et al., 1991; Skinner et al., 2008). Discrete OES and EDJ traits were evaluated and compared to published databases on Neandertals and Upper Paleolithic modern humans (Bailey, 2002a, b, 2006; Bailey et al., 2011; Martinón-Torres et al., 2012, 2014; Martínez de Pinillos et al., 2014; Martin et al., 2017; Scott and Irish, 2017; Davies et al., 2019; SOM Tables S2–S5).

Maximal root length for the dental description was taken preferentially from the buccal side of the tooth, perpendicular to the occlusal surface, from the cervix to the apex or fractured end of the root. For crown metric analyses, conventional mesiodistal and buccolingual diameters were measured twice each by J.H. and B.M. (means given in SOM Table S6), using 150-mm Mitutoyo digital calipers (0.01-mm accuracy; Martin and Saller, 1957; Hillson, 1996). Teeth displaying significant taphonomic alterations (mechanical degradations or biocorrosion) and/or severe occlusal wear were excluded from the metric comparisons. Bivariate scatterplots were generated in R v. 4.2.2 (R Core Team, 2022), with 'ggplot2' v. 3.5.1 (Wickham, 2016), to consider the Grotte du Bison specimens within the Eurasian Neandertal and Middle Pleistocene human variability (SOM Table S3). Moreover, confidence ellipses of 95% were generated relative to the distribution of a Holocene modern human sample.

Additional analyses were conducted on the paired specimens, as described in SOM S1 methods.

3. Results

3.1. Cranial and postcranial collection

All the cranial and postcranial fragments described below belong to adult individuals (Fig. 3).

Left parieto-occipital fragment #47 This cranial piece (Table 2; Fig. 3) comprises a left parieto-occipital fragment located medially from the asterion and mastoid angle. The inferolateral part of the external occipital surface shows signs of taphonomic erosion, but the endocranial surface is well preserved. In the medial part of the fragment, calcite crystals developed in the lambdoid suture (open arrow, Fig. 3). On and below the protruding part of the torus relief, four subparallel scratches (10 mm long) are observed, likely caused by taphonomic trampling processes (contrary to cut marks, e.g., Les Pradelles occipital bones in Mussini, 2011). The thickness of the two cranial bones suggests they belong to a mature cranial vault.

The occipital part (48.26 × 34.15 mm) is interlocked with a smaller parietal fragment (31.29 × 23.78 mm). Laterally from the lambdoid suture, a partially synostozed small supernumerary bone is present on the occipital bone (as in the El Sidrón 'SD 1219' occipital bone; Bastir et al., 2010). Laterally from the occipital fragment, a 3 × 5 mm–long portion of the occipitomastoid suture is preserved. The occipital fragment shows the external muscular insertions on the nuchal plane and a clear relief representing the lateral end of an occipital torus (bounded by the superior and inferior nuchal lines).

A convexity is expressed at the sutures. Inside the cranium, the meninges are strongly marked. The transverse (sigmoid) sulcus, present distally on the parietal fragment, is deep and curved (as in Las Pelenos Neandertal, France; Scolan et al., 2012).

Right temporal bone fragment #48 This triangular cranial fragment (Table 2; Fig. 3) has well-preserved bone surfaces, with minimal external taphonomic erosion, except for the oblique fractures located medially on the superior edge of the endocranial face and the inferior edge of the external face.

We consider this fragment (33.5 × 27.5 × 21.0 mm) to be the posterior part of the right temporal bone of a mature individual, with the thickness and morphology of the asterion, showing an 18-

Table 2
Skeletal collection from the Grotte du Bison, including specimen number, fieldwork label (indicating site 'A' for Arcy-sur-Cure followed by the year of discovery, cave 'B' for Grotte du Bison, the archaeological layer [by stratigraphic unit], location, and sometimes a specimen number, according to the discovery), stratigraphic unit, and the identification of the remains.

Specimen ID	Fieldwork label	Archaeological layer	Skeletal fragments
47	A2010 B I R11 10	I	Right occipital and parietal
48	A2010 B I O/Q12 1	I	Right occipital
49	A2010 B I O9	I	Parietal
50	A2010 B I Q 10 30	I	Right parietal
51	A2010 B I R12	I	Left parietal
52	A2011 B I O10 244	I	Left parietal
(53)[a]	A2010 B I T12 20	I	(Right rib)
54	A2019 B J2 R12 31	J	Right fibula
(55)[a]	A1963 B J U14 356	J	(long bone)

ID = identification number of the specimen in our study.
[a] Described with SOM Fig. S1, with the uncertainties regarding their taxonomic status.

mm segment of the parietomastoid suture and a 20.5-mm segment of the occipitomastoid suture. Large neurovascular bundles create large indentations in the parietomastoid suture, just below the asterion (similar to La Quina H5), more commonly seen as foramina expressed to the side of the parietomastoid suture (e.g., La Chapelle-aux-Saints 1). On the endocranial surface, we observe the eroded posterior extremity of the petrous pyramid, lacking protrusion. Below, the sigmoid sulcus is deep and superiorly convex. Finally, a small foramen is present medially from the latter structure.

Frontal or parietal fragment #49 This small triangular cranial fragment (37.5 × 32.0 × 28.0 mm) exhibits the morphology of both external and internal compact tables, as well as diploë, consistent with a human skull fragment (Table 2; Fig. 3). The fragment is 6.5 mm thick, in the range of mature cranial vault thickness.

Figure 3. Cranial and postcranial fragments from the Grotte du Bison: the external and internal views of the right occipital and parietal fragment #47; right occipital fragment #48; parietal fragment #49; right parietal fragment #50; left parietal fragment #51; left parietal fragment #52; and the anterior and posterior views of the right fibula fragment #54 (Table 2). Scale bar = 1 cm.

The fragment displays taphonomic wear, with cracks on the external side and half of the endocranial surface missing, exposing the diploë. There is no external curvature of the fragment. On the preserved portion of the endocranial side, the imprint of neurovascular grooves and irregular topography resembles the lower aspects of the parietal or frontal bones.

Parietal fragment #50 The cranial fragment (Table 2; Fig. 3) is nearly square in shape (387.9 × 363.6 mm) and exhibits significant loss of bone surface on the external side. The morphology of the external and internal compact bone tables, along with the diploë, is characteristic of a mature human skull. Furthermore, this fragment is notably thick (9.0 mm at the middle of the piece).

The preserved endocranial side with meningeal grooves allows for its identification as a parietal fragment, but it does not permit lateralization of the bone with certainty. Distinctive meningeal grooves branch out and are oriented in a superoposterior direction, running nearly parallel to two other, less deeply printed meningeal grooves within the internal table. This pattern could be seen on a right parietal fragment. This morphology situates the fragment in the anterior section of the parietal bone, above the sphenoid angle and superoposterior to the anterior ramus. The remaining portion of the external side, constituting approximately half of the fragment surface, displays a discernible smooth relief identified as the superior temporal line. Based on this evidence, we propose that this fragment could be a right parietal bone.

Parietal fragment #51 This small cranial fragment (Table 2; Fig. 3) is trapezoidal in shape (25.08 × 245.04 mm). A fifth of the external surface is preserved, in contrast to the almost intact endocranial side. Its thickness reaches 8 mm, consistent with mature cranial bones. The endocranial face presents an embossed surface topography. Its meningeal network, with three deeply printed grooves, is superoposteriorly oriented. This morphology likely corresponds to the central and/or lower region of a possibly left parietal bone, in the area of the posterior ramus of the meningeal vessels.

Left parietal fragment #52 This fragment (Table 2; Fig. 3) seems rhomboidal in anatomical position (61.5 × 41.0 mm), with an angled fracture and two sutures, respectively, on the left and right of the external face. Considering its suture morphology, this piece corresponds to the posterior superior angle of a left parietal bone. The well-preserved sagittal suture is 38.0 mm long, whereas the lambdoid suture is 31.0 mm long and more worn. The worn inion on the right side of the external face suggests a left lateralization of the parietal fragment. The lambda area is slightly eroded, but the presence of a supernumerary lambdoid sutural bone is suspected in the inferior part of the fragment. The external and internal compact bone surfaces present a few fine taphonomic cracks. The fragment appears flat, but such lack of curvature may result from slight postdepositional plastic deformation and/or may be influenced by the size of the fragment. As the fragment is 7.5 mm thick at its center, it is considered to be a mature cranial bone.

Although there are no imprints of the meningeal networks, a relatively smooth and low ridge is expressed along the sagittal sulcus.

Right fibula fragment #54 The fibula was broken in two pieces upon discovery (Fig. 3, open arrows); they were found close to each other and were easily refitted (labeled identically, with '1' for the proximal part and '2' for the distal part), forming a 208.0-mm-long diaphysis fragment (Table 2; Fig. 3). There is manganese coloration on the entire bone surface, especially the proximal end. The distal fragment was sampled for isotopic analyses (<200 μg, over less than 1 mm^3; Dodat et al., 2024).

The main nutrient foramen is large and located on the posteromedial crest, opening 95 mm below the preserved proximal end of the diaphysis, with a 17.5-mm-long groove (Fig. 3, plain white arrows). The medial side is slightly convex, whereas the posterior side ranges from flat to slightly convex, featuring short lateromedial oblique crests. A crest distinctly separates the posterior side from the medial side. The proximal two-thirds of the lateral view are deeply concave (Fig. 3b), and it is also clearly delineated from the medial and posterior views by well-defined crests. The anterior interosseous crest is strongly expressed (Fig. 3a), with a flat and coarse proximal surface, probably an enthesopathy.

3.2. Deciduous teeth

Right dI^1 #7 The tooth is almost complete (Table 1; Fig. 4; David et al., 2009; Tillier et al., 2013a), but the crown was significantly broken since the Tillier et al. (2013a) study. Most of the occlusal edge and distal marginal ridge are now missing. Furthermore, the root presents a taphonomic perforation labially but is overall well preserved (10.4 mm of root length). Contrary to Tillier et al. (2013a), our assessment indicates that the tooth is functionally worn on the preserved incisal edge (occlusal wear: stage 2; Table 1) and that the root apex is not fully closed. Furthermore, the lingual enamel is worn down, probably due to lingual attrition. Thus, this individual likely died during infancy (ca. 1.5 year).

The root is slightly concave labially and wider buccolingually. Finally, as Tillier et al. (2013a:p. 42) noted with radiographs of the tooth, the pulp cavity is enlarged compared to the dentine thinness of the root (Fig. 4). The crown exhibits a noticeable labial convexity. The remaining marginal ridge is elevated. Tillier et al. (2013a:p. 42) described the still incomplete crown as shovel shaped.

The EDJ reflects the OES morphology, with a less pronounced cingulum and a distal flattening of the labial convexity of the crown.

Left dC^1 #15 The tooth crown is complete (Table 1l; Fig. 4; Tillier et al., 2013a), but the root presents significant taphonomic degradation, with only a few cement patches remaining mesially and distally. Nevertheless, this taphonomic erosion does not significantly impact the overall root length (8.53 mm) but supposedly widened a resorbed root apex. The crown is functionally worn (Stage 5; SOM Table S3), with a wear basin subhorizontally following the mesial marginal ridge and another wide distal wear basin oriented buccolingually. Additionally, the lingual side of the crown is chipped distally, and an important pitting is seen at the occlusal surface, particularly lingually and near the cingulum. We consider that this individual might have died during preadolescence (8.5–10.5 years).

The short root has a proportionally wide circumference, but the pulp cavity is relatively thin (its diameter being half as large as the dentine thickness of the root; Fig. 4).

The cervical margin of the crown is bulbous and asymmetrical, with the buccal margin tapering distally. A marked distal 'pinching' is observed on the marginal ridge, influenced by the distal interproximal contact facet (Fig. 4).

At the EDJ, only the mesial marginal ridge is preserved, distinctly separated from the cingulum by a marked intervening 'pinch' of the ridges.

Left dP^4 germ #1 This tooth was not in occlusion (Table 1; Fig. 5; Tillier et al., 2013a), as the crown is unworn, and the broken roots are not fully developed (3.01 mm). This individual probably died during infancy (1.5–2.5 years).

The tooth features five cusps with inward-oriented apices, including four main cusps (Pa > Pro > Met > Hyp) and a reduced distobuccal accessory cusp, connected by a narrow marginal ridge. The oval-shaped occlusal basin is oriented buccomesially to distolingually. The central sagittal sulcus leads to a faintly expressed anterior fovea on the Pa (grade 2; SOM Table S5a), whereas the Pro presents a mesial accessory ridge. An accessory tubercle is expressed

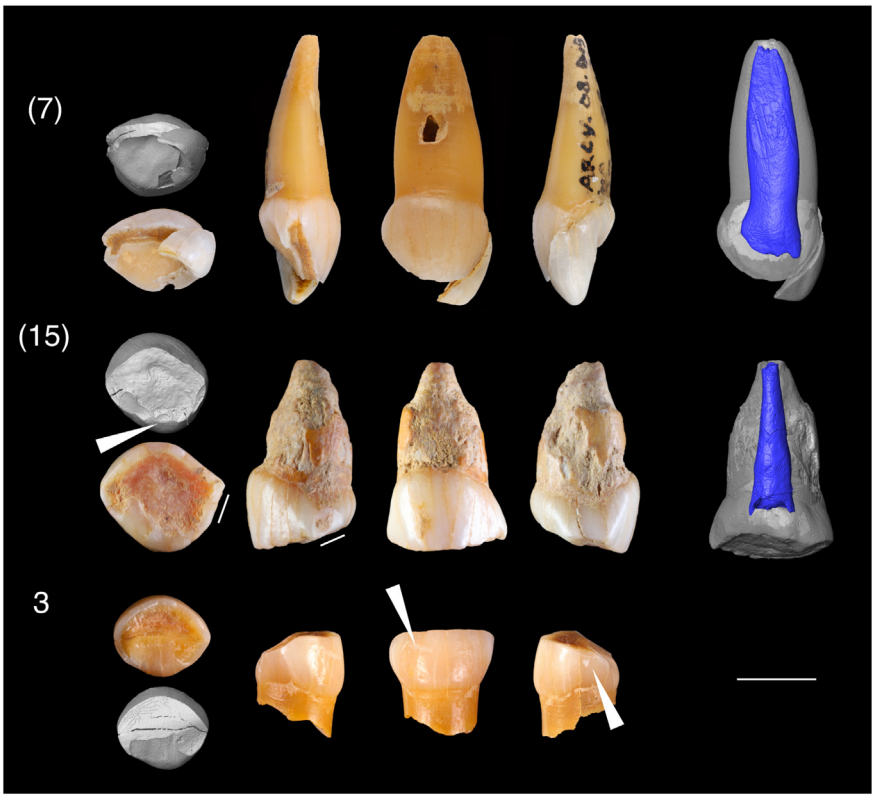

Figure 4. Deciduous anterior teeth from the Grotte du Bison: RdI^1 #7; LdC^1 #15; RdC_1 #3 (Table 1); with the OES and the EDJ in occlusal, distal, labial, and the lingual views (every view in SOM Fig. S2a), with the pulp cavity of #7 and #15 in buccal and lingual views, respectively. On canine #3, the arrows indicate hypomineralized enamel spots on the crown, and on #15, the arrow indicates the isolated tuberculum dentale. The parentheses show the previously published teeth. Scale bar = 5 mm. EDJ = enamel–dentine junction; OES = occlusal enamel surface.

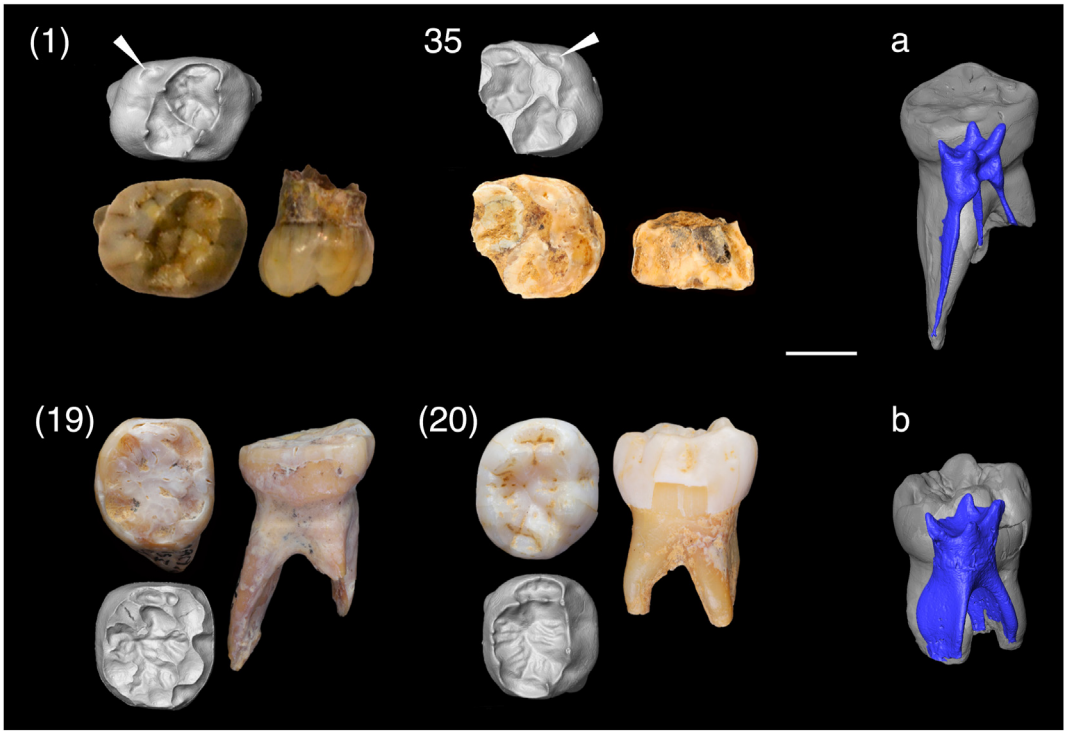

Figure 5. Deciduous premolars from the Grotte du Bison: LdP^4 germ #1; RdP^4 #35; RdP_4 #19; RdP_4 #20 (Table 1), with the OES and the EDJ in occlusal and distal views (every view in SOM Fig. S2a). The pulp cavities of the LLdP4s #19 and #20, respectively, (a) and (b), are shown in buccodistal views. The white arrow indicates Carabelli expressions on #1 and #35 EDJ. The parentheses show the previously published teeth. Scale bar = 5 mm. EDJ = enamel–dentine junction; OES = occlusal enamel surface.

distally from the Pro, and a tubercle-like structure is expressed mesially from the Met. A Carabelli's tubercle is present with a marked Y-shaped furrow (grade 4; SOM Table S5a; arrow in Fig. 5).

At the EDJ, the dentine horns are high in comparison to the marginal ridge, especially as it flattens at the distal dentine horns and distally from the Pro. Both the Pa and Met exhibit distal accessory horns. The continuous crista obliqua (grade 1; SOM Table S5a) is marked by an accessory dentine horn on the Pro distal accessory ridge, and an accessory ridge is expressed mesially from the Met, oriented toward the Pa. A faintly expressed ridge defines the distal border to the shallow anterior fovea (grade 2; SOM Table S5a).

Right dP^4 #35 The tooth is highly degraded (Table 1; Fig. 5). Only a trampled portion remains, representing two-thirds of the lingual part of the crown. Pronounced occlusal wear created substantial dentine patches on each cusp (stage 5; Table 1). The individual likely died during preadolescence (9.5–11.5 years).

Among the cusps, only the Hyp and Pro are complete, with the Hyp nearly as large as the Pro. An accessory tubercle is observed on the distal marginal ridge between the Hyp and Met. The sagittal sulcus appears to be divided by a crest connecting the Pro and Met. An anterior fovea is expressed near the Pa (grade 1; SOM Table S5a), and a mesial sulcus is visible on the Pro mesial side.

At the EDJ, the ridging in the occlusal basins is not highly complex and the crista obliqua is continuous (grade 1; SOM Table S5a). The anterior fovea is expressed with a mesial lateral accessory ridge of the Pa that flattens into the Pro mesial marginal ridge (grade 2; SOM Table S5a). Another fovea is present on the crown wall, lingually from the mesial marginal ridge, and similar to a Carabelli expression not visible at the OES (arrow, Fig. 5).

Right dC_1 #3 The tooth was lost antemortem (Table 1; Fig. 4), during late childhood (ca. 7.5–10.5 years), as its root is almost fully resorbed (2.68 mm buccally and >1 mm lingually). Hypocalcification areas are observed on the crown, labially and on the mesial marginal ridge. The occlusal wear (stage 4; Table 1) extends to the cingulum with a considerable occlusal facet, a separate a small plane is present mesially, and a gully-like facet (heavily pitted on the enamel edge) distally. On the labial side, the enamel surface is pitted, especially distally. Oblique striae are also visible.

The crown and root outlines are rounded, and the distal asymmetry of the crown is well expressed. However, the labial side of the crown lacks convexity and bulbous cingulum, contributing to the overall gracile aspect of the tooth.

The mesial marginal ridge is noticeable at the EDJ and blends into a less defined cingulum.

Right dP_4 #19 The tooth is deteriorated (Table 1; Fig. 5; Tillier et al., 2013b). It has undergone significant acidic deterioration, probably due to partial digestion by a carnivore (Maureille et al., 2017), with no remaining trace of cementum and an important loss of dentine and enamel, and an important cervical erosion. In addition, half of the mesial root was broken. There is no clear evidence of apical resorption on the preserved distal root. The crown displays heavy occlusal wear (stage 5; Table 1) and a prominent mesial contact facet. Thus, this individual likely died during late childhood (6.5–8.5 years).

The mesial root pulp is separated in two sections, and the single distal root presents an extended pulp cavity laterally (Fig. 5a). The crown exhibits a rounded shape on the lingual and distal sides, with flattened buccal and mesial sides. A pronounced buccal intercuspal fossa is present. The occlusal morphology can be inferred from the sulcus and enamel contours. The mesial cusp appears to have small distal accessory ridges, whereas the Hyp, C5, and Ent exhibit highly complex structures. Mesial ridges on the Pro and Met form a continuous distal border for the anterior fovea, which appears interrupted on the buccal side.

At the EDJ, the occlusal complexity is important, with high accessory ridging on the main cusps and on a suspected C7. Additionally, the anterior fovea is interrupted by a small ridge, and an accessory ridge is observed on the distobuccal border.

Right dP_4 #20 The tooth is well preserved (Table 1; Fig. 5; Tillier et al., 2013b), aside from a rectangular enamel break centered in the lower half of the buccal crown wall (present in Tillier et al., 2013b). There is also some taphonomic pitting on the tooth and especially on the roots. The fused and dissociated root portions are equivalent, with broken and unfused apices (maximal root length = 7.58 mm). The mesial root also presents dissociated pulp canals apically (Fig. 5b). Given the absence of occlusal wear, we conclude that the tooth was not fully developed, rather than being a preadolescent tooth with resorbed root apices as suggested by Tillier et al. (2013). Therefore, this individual most likely died during infancy (1.5–2.5 years).

The rounded crown presents five isolated main cusps (Ent ≥ Pro > Met ≥ Hyp > C5) but a hardly discernible occlusal complexity. The distal accessory ridge of the Pro is dissociated from its apex and aligned with the deep intercuspal groove. The Met essential crest is distally bifurcated. The Ent and C5 exhibit complex features, whereas the C6 and C7 are faintly expressed. The anterior fovea is marked (grade 3; SOM Table S5a), with the Pro and the Met forming a marked distal border, interrupted by the narrow onset of the sagittal sulcus. Faintly expressed ridges are present on the mesial marginal ridge bordering tubercular expressions. Additionally, a distal fovea is formed by lateral ridges of the Ent and C5, with an interrupted mesial border by the sagittal sulcus.

At the EDJ, the ridging is more discernible. Accessory dentine horns are marked on the Met mesial lateral ridge and Pro essential crest, connecting sagittally into an uninterrupted distal border to the anterior fovea. The C7 and distal accessory ridge to the Met are nearly identical. Finally, the C6 is faintly expressed by the uninterrupted distal marginal ridge that borders the wide distal fovea.

3.3. Permanent teeth

Left I^1 #11 Only an incomplete crown remains from this taphonomically broken tooth (Table 1; Fig. 6; Tillier et al., 2013a). The cervical edge of the crown is missing labially, whereas the cingulum is chipped lingually. Less than a millimeter of root is preserved mesially and distally. The crown exhibits minimal occlusal wear (stage 2; Table 1), but the distal half of the incisal edge is notched. This individual died at least during the prepubertal period (8.5–11.5 years).

The crown displays a distinct shoveling (stage 4; SOM Table S2) and features a convex labial surface (grade 4; SOM Table S2). The marginal ridges are well defined, especially the distal marginal ridge, which is isolated from the lingual structures by a deep sulcus. The tuberculum dentale (grade 4; SOM Table S2) is expressed as two large ridges separated by a shallow sulcus that fades at the cingulum.

The marginal ridges are similarly expressed at the EDJ (grade 4 for labial convexity; grade 2 for shoveling; grade 2 for tuberculum dentale; SOM Table S2). However, there is significant lingual complexity with numerous small accessory ridges. Additionally, the apical half of the labial side is slightly concave, possibly associated with a reduced double-shoveling expression (grade 1; SOM Table S2), absent from the OES.

Left I^1 #45 This tooth is complete (Table 1; Fig. 6), but fractures have expanded since its excavation in 2019 (a frontal fracture of the root and four fractures on the crown are visible on the distal and buccal sides). A pit is evident at the center of the labial surface, near the incisal edge, and probably corresponds to a developmental defect (Fig. 6a). A substantial patch of supragingival calculus is also noticeable on this surface. Slight apical hypercementosis is present

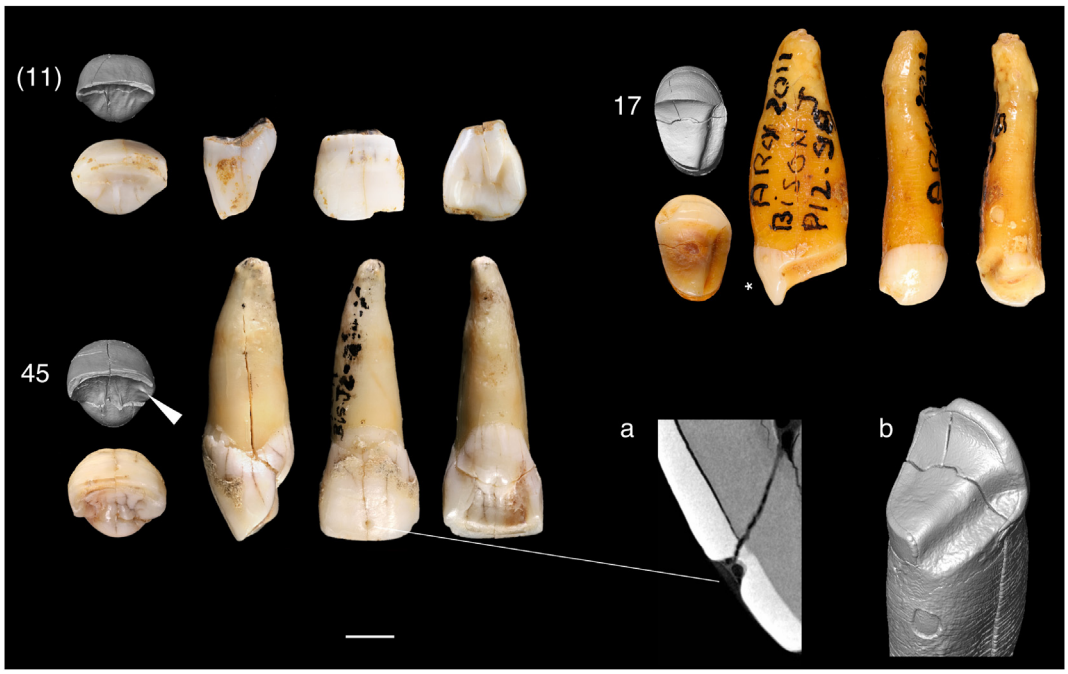

Figure 6. Upper permanent incisors and canines from the Grotte du Bison: LI^1 #11; LI^1 #45 and (a) a sagittal plane of its lingual deformation; LC^1 #17 and (b) its distal wear (Table 1); with the OES and the EDJ in occlusal, distal, labial, and lingual views (every view in SOM Fig. S2b). The arrow indicates a distal accessory tubercle (#45). The asterisks indicate linear hypoplasic events. The parentheses show the previously published. Scale bar = 5 mm. EDJ = enamel–dentine junction; OES = occlusal enamel surface.

on the root (length = 16.21 mm). The occlusolingual wear exposes a continuous dentine line, extending to the extremities of the marginal ridges (stage 3; Table 1), also affected by large interproximal facets. Consequently, the estimated age at death falls within a range spanning from the prepubertal to early adolescence period (8.5–11.5 years).

The tooth's profile appears convex, with the crown and root apices converging toward the lingual side (defined in the French literature as 'cyrtodonte'; Patte, 1962). The crown displays marked shoveling (grade 5; SOM Table S2) with a moderate labial convexity (grade 4; SOM Table S2) and markedly developed marginal ridges. The distal marginal ridge is two times bigger than the mesial one, with a wider sulcus. Deep lateral sulci also isolate the marginal ridges from the pronounced tuberculum dentale (grade 4; SOM Table S2), expressed with two ridges in the lingual convexity. Furthermore, the mesial marginal ridge presents a shallow mesial interruption groove.

On the EDJ, the shoveling is well expressed (grade 4; SOM Table S2). The labial convexity is slightly more pronounced (grade 4; SOM Table S2). The two ridges of the tuberculum dentale are neatly discernible. Additionally, a subhorizontal accessory ridge is present midway through the distal marginal ridge (Fig. 4), contributing to the pneumatized aspect of the ridge at the OES.

Left C^1 #17 The canine is well preserved despite the taphonomic crackling that extends throughout the cementum (Table 1; Fig. 6). Small calculus patches are present on the buccal side and distally, above the cingulum. Approximatively 2 mm from the apex of the crown, a large and shallow linear concavity or hypoplasia is observed (Fig. 6). Furthermore, about a third of the root exhibits apical hypercementosis (7.1 mm of a 21.6-mm-long root). The root, initially narrow and concave toward the mesial side, is enlarged mesiodistally when viewed from the buccal side. The entire lingual surface of the tooth is functionally worn (stage 4; Table 1), revealing the pulp cavity filled with tertiary dentine. A duct-like wear pattern is evident on the entire distal side of the crown (Fig. 6b), distinct from regular occlusal attrition patterns. In the buccal view, a notch is marked mesially by two large enamel chips (grade 3; Belcastro et al., 2018). This individual was at least middle-aged at death.

The lingual profile of the tooth is highly convex (cyrtodont), with a well-rounded root contour (in lateral view) enhanced by the apical hypercementosis. In the transverse view, the root is shaped like an '8.'

Right P^3 #33 The tooth crown is almost intact (Table 1; Fig. 7), but the roots are badly preserved. Approximately half of the mesial root is present (about 10 mm on the buccal side and 6 mm on the lingual side), and the distal side is worn up to the crown cervix. The perikymata of the crown are clearly visible, along with subtle hypoplasic pitting and a pronounced linear hypoplasia in the first third of the crown's height (evident buccally). The crown shows minimal wear, with facets inside the Pa marginal ridges and distally on the Pro and distal accessory cusp (stage 2; Table 1). Furthermore, an interproximal contact facet is present distally. This individual probably died early during adolescence (ca. 12.5–14.5 years).

On the remaining portion of the root, a prominently marked mesial groove extends up to the crown. The crown exhibits a slight asymmetry when viewed from the occlusal perspective, with the distal features being more prominent. The Pa marginal ridges form distinct angular protrusions, leading to lateral sulci and accessory tubercles mesially and distally. The Pro is globular, featuring a mesially placed bifurcated essential crest, aligned with the essential crest of the Pa (grade 2 for the Pro; grade 1 for the Pa; SOM Table S3). The deep sagittal sulcus separates the crests (grade 0 for the transverse crest; SOM Table S3).

At the EDJ, there is a noticeable mesial concavity that extends from the wide radicular groove up to the crown. At the occlusal surface, the essential crest remains continuous (grade 2; SOM Table S3), even as it follows the topography of the cusps. A thin distal lateral ridge characterizes what is seen as the Pro's essential

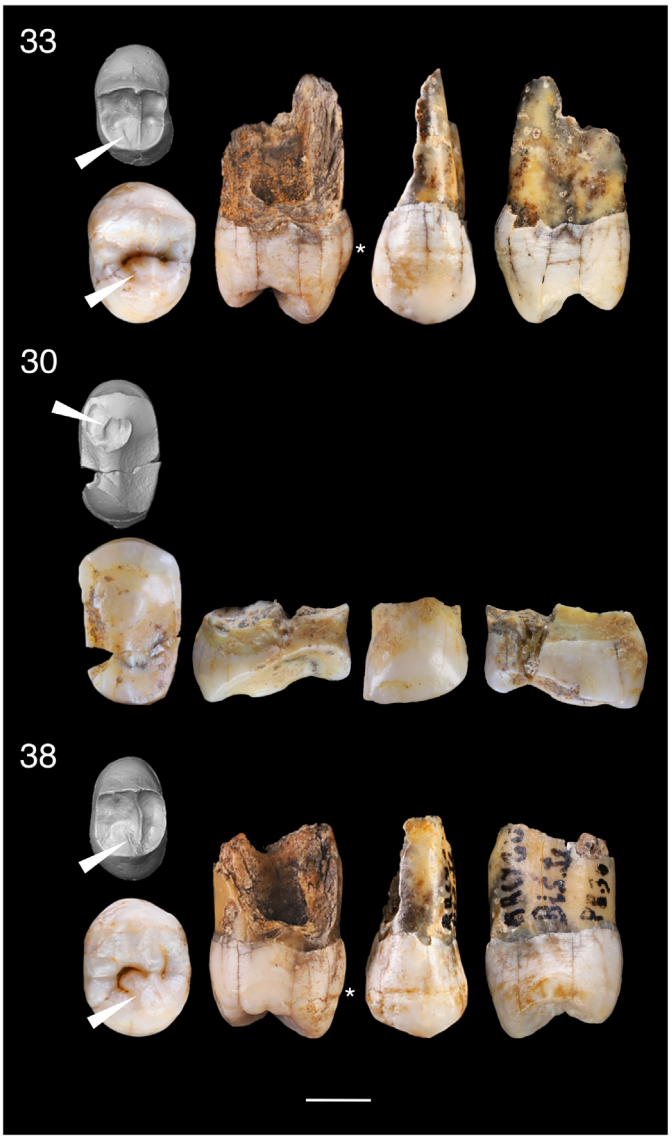

Figure 7. Upper premolars from the Grotte du Bison: RP^3 #33; LP^4 #30; RP^4 #38 (Table 1); with the OES and the EDJ in occlusal, distal, buccal, and mesial views (every view in SOM Fig. S2c). The arrow indicates the buccal essential crest of the tooth #30; the bifurcated crests of #33 and #38. The asterisks indicate linear hypoplasic events (on #33 and #38). Scale bar = 5 mm. EDJ = enamel–dentine junction; OES = occlusal enamel surface.

crest bifurcation at the OES (grade 1; SOM Table S3). On the Pa, a distal thickening of the occlusal basin and a slight accessory dentine horn expressed on the marginal ridge form a distal accessory ridge (grade 1; SOM Table S3), absent from the OES. The accessory tubercles are not clearly expressed at the EDJ. The mesial marginal ridge presents a central pinching, and the distal marginal ridge shows a slight thickening, above the central sulci.

Left P^4 #30 This tooth is poorly preserved (Table 1; Fig. 7). The crown is broken in two main pieces, with a pyramidal fragment missing mesially (leaving a triangular gap in occlusal view). The root(s) is (are) broken with about a millimeter preserved above the cervix. The partially preserved tooth displays severe wear (stage 6; Table 1), with only an enamel patch remaining on the Pa. There is an oblique wear basin in the mesial half of the crown and a broader one on the distal side. The presence or absence of a distal interproximal contact facet cannot be confidently assessed, but the mesial one is well visible and extends over the mesial side of the crown. These wear characteristics suggest that this individual is likely an older adult.

The crown is notably large (11.8 mm buccolingually; SOM Table S6), with a rectangular outline mesiodistally and seemingly thick enamel.

The EDJ supports the lateralization of the tooth as it exhibits a mesially placed ridge that defines the interrupted distal border of an anterior fovea. Moreover, both the mesial and distal sides on the buccal aspect feature superoinferior convexities.

Right P^4 #38 The crown is nearly complete, and approximatively half of the root is preserved (ca. 8.8 mm) on the mesial side (Table 1; Fig. 7). The distal portion of the root is missing up to a millimeter near the cervical line. Small enamel chips are absent from both the buccal and lingual edges of the cervix. The crown exhibits pronounced hypoplasic defaults, particularly on the buccal face, above a significant linear hypoplasia marking the upper half of the crown. Occlusal wear is limited to a small facet distally on the apex of the Pa essential crest and to a smoothed edge lingually from the Pro apex (stage 2; Table 1). This individual likely died early in their adolescence (ca. 13.5 years).

The root section is oval and lacks significant mesial concavity. The crown outline is fairly rectangular and bulbous. The marginal ridge is continuous and appears pneumatized, featuring two distal tubercula (with deeper sulci on the lingual one) as well as a slight distal accessory ridge on the Pa (grade 1; SOM Table S4). There is also a central tuberculum on the anterior fovea mesial marginal ridge, with a shallow separation groove. With these marginal structures, the anterior fovea is narrow but well defined. The essential crests of the main cusps (grade 1 for the Pa and grade 2 for the Pro; SOM Table S4) join mesially to form a nearly uninterrupted distal border to the anterior fovea (grade 1 for the transverse crest; SOM Table S4). The sagittal sulcus is crescent-shaped, opening toward the Pro distal bifurcation (grade 2; SOM Table S4).

At the EDJ, the marginal ridge remains continuous, with a rounded mesial section and a more squared distal portion, widening distolingually. The transverse crest is also uninterrupted but dips at the sagittal fissure (grade 2; SOM Table S4). The distal lateral accessory ridges are prominently visible compared to the deep sulci. The Pa distal accessory ridge is short and faintly expressed (grade 1; SOM Table S4), contrary to the Pro distal bifurcation (grade 2; SOM Table S4), both expressed as on the OES.

Left M^1 germ #6 This tooth germ has undergone significant taphonomic alteration, likely mechanic erosion, on the entirety of the enamel surface (Table 1; Fig. 8; David et al., 2009; Tillier et al., 2013a). On the crown walls, the enamel is worn out to the dentine surface (distally from the Hyp and buccally from the Pro). However, the crown was not fully developed, and the individual died during early childhood (ca. 2.5–3.5 years).

The crown outline is square. The lingual side presents more developed accessory ridging, with a cusp-like distal accessory ridge to the Pro and a large distal accessory ridge to the Hyp. The Met essential crest joins the buccal side between the essential crest of the Pro and its cusp-like distal accessory ridge.

The crown morphology is entirely preserved at the EDJ. The marginal ridge is continuous, drawing a wide occlusal basin. Four accessory dentine horns are expressed on the marginal ridge. A dentine horn is expressed with the central accessory ridge on the mesial marginal ridge. The Pa and Met distal accessory ridges also present dentin horns at the marginal ridge, as well as the C5 expression distally. The Pro distal accessory ridge and the C7 essential crest do not induce any accessory dentine horn on the marginal ridge. Both the Pro and the Pro distal accessory ridges present mirroring ridges on the lingual wall. The crista obliqua is

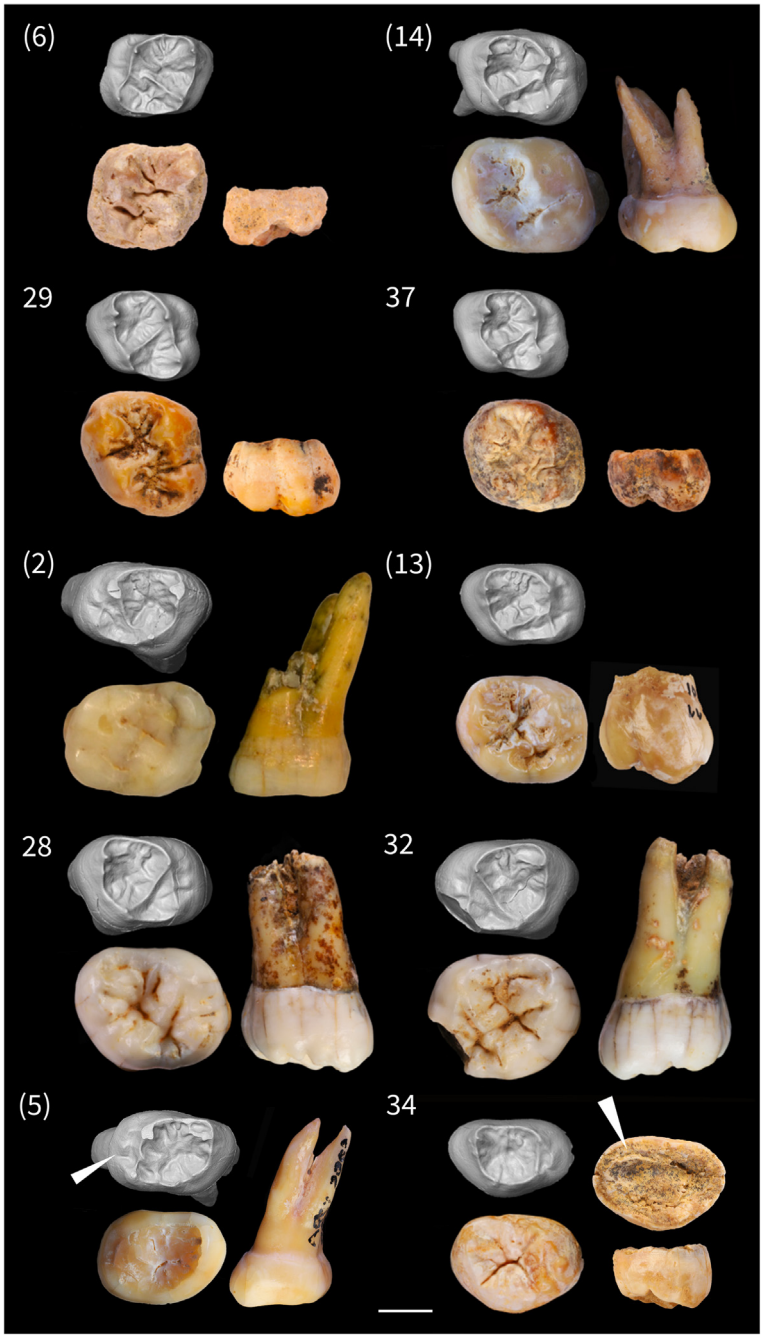

Figure 8. Upper permanent molars from the Grotte du Bison: LM^1 germ #6; RM^1 #14; RM^1 germ #29; RM^1 #37; LM^2 #2; $RM^{2/3}$ germ #13; $RM^{2/3}$ #28; $LM^{2/3}$ #32; LM^3 #5; RM^3 germ #34 (Table 1); with the OES and the EDJ in occlusal and distal views (every view in SOM Fig. S2d). The arrow indicates an accessory tubercle on the #5 lingual wall and the pulp cavity of #34. The parentheses show the previously published teeth. Scale bar = 5 mm. EDJ = enamel–dentine junction; OES = occlusal enamel surface.

expressed by the Met essential crest that flattens into the Pro distal accessory ridge, drawing a distal wrinkling (grade 0; SOM Table S5b). A distal bifurcation is present midway through the Met essential crest and joins the accessory ridging of the distal margin, circling a buccodistal tubercle.

Right M^1 #14 The tooth is complete but exhibits signs of acidic alteration and/or has been partially digested by a carnivore (Table 1; Fig. 8; Tillier et al., 2013a). The enzymatic alteration is not as significant as in #19, but the overall surface of the tooth is highly glossy, there is significant cementum and dentine loss, and the root apices are opened (as #5). The mesiobuccal root is partially broken. The tooth was functional (stage 2; Table 1), and interproximal contact facets discerned the mesial and distal flattening of the crown walls. Thus, the tooth likely belonged to an older adolescent or young adult (16.5–20.5 years).

The molar is three rooted (ca. 11.36 mm) and without notable pulp cavity extension (SOM Fig. S4). The crown has a square/trapezoid outline, with a prominent Pro and a Hyp larger than the Met

(Pro > Pa ≥ Hyp > Met). The Pro and Met are connected, whereas the Pa and Hyp are isolated by wider sulci. A C5 and a distal accessory ridge to the Pa are expressed.

At the EDJ, the marginal ridge is interrupted at the Hyp, which is isolated from the cusps with a deep sulcus marked distally from the crista obliqua (continuous from the Met to the Pro distal accessory ridge; grade 0; SOM Table S5b). The separate marginal ridge of the large Hyp joins the complexity on the lingual buccal face. The Hyp expression and wide occlusal basin are characteristic of the first molars. The buccal horn tips are directed inward. Both the Pa and Met exhibit a distal accessory dentine horn. Accessory dentine horns are also present on the mesial and distal marginal ridges; these are buccally situated and without any ridging at the occlusal basin. The distal one is well defined and isolated and corresponds to the C5 expression at the OES. Additionally, two tubercular ridges are expressed mesially. Finally, the Pro lingual wall is ridged.

Right M^1 germ #29 This tooth germ is fully developed up to the cervix (Table 1; Fig. 8), and there is no evidence of root development regardless of the slight taphonomic erosion of the cervix. The crown displays slight taphonomic pitting and noticeable trampling marks on the lingual side. Also, the enamel appears ocher, with a darker coloration on the cusp tips. The individual died during early childhood (ca. 3.5 years).

The crown's outline is highly asymmetric, with the mesial marginal ridge protruding buccally and the distal tuberosities connecting to a lingually positioned Hyp (Pro > Pa > Met > Hyp; SOM Table S5b). The Hyp is well isolated, and the distal accessory structures contribute to a longer mesiodistal diameter compared to the buccolingual one. The Pro distal accessory ridges are isolated from the main cusp, and they are separated by the complex essential crest of the Met. Both buccal cusps exhibit small distal accessory ridges. The three mesial and distal accessory tubercular ridges (mesial marginal accessory tubercles; grade 1; SOM Table S5b) converge at the sinuously expressed sagittal sulcus.

At the EDJ, the marginal ridge is rounded mesiobuccally and distolingually. Accessory dentine horns are present on the mesial marginal ridge, and each lingual cusp has a distal accessory dentine horn corresponding to the distal accessory ridges at the OES. A slight horn is also present on the marginal ridge above the two distal accessory ridges of the Pro. The crista obliqua is formed by the Met essential crest, which flattens distally from the Pro crest (grade 0; SOM Table S5b). The occlusal basin is complex on both sides.

Right M^1 germ #37 This tooth germ is not fully developed (Table 1; Fig. 8), with its cervical edge mechanically eroded. Overall, the crown surface shows taphonomic pitting similar to trampling impacts. If we consider that the tooth is a first molar, the individual died during adolescence (ca. 3.5 years).

The crown outline appears square, with a slight mesiodistal elongation, and a distal asymmetry induced by a reduced Met compared to the Hyp expression (Pro > Pa > Hyp > Met; SOM Table S5b). The mesial cusps have mesial accessory ridges that converge into the sagittal sulcus and embrace central accessory tubercles on the mesial marginal ridge (mesial marginal accessory tubercles; grade 1; SOM Table S5b). The distal accessory ridges to the Pa and Pro are cusp-like. Moreover, the sagittal sulcus has a sinuous appearance and is interrupted by the complex Met ridging that joins the Pro distal accessory ridge.

At the EDJ, the marginal ridge forms a notch at the Hyp. Mesially from this buccal ridging, a deep groove is continuous with the Pro distal accessory ridge. The Pro also presents a marked concavity on the buccal wall. The crista obliqua is expressed with the Met essential crest, which flattens between the Pro essential crest and the distal accessory ridge (grade 2; SOM Table S5b). Distal accessory dentine horns are associated with faint ridges on the Pa and Met. Additionally, accessory dentine horns are present mesially on the Met, with slight ridges on the mesial marginal ridge. The buccal cusp horn tips are directed inward.

Left M^2 #2 The tooth is complete except for the fractured mesiobuccal root (Table 1; Fig. 8; Tillier et al., 2013a). Furthermore, there are noticeable molding traces present over the root's cracks and grooves. The crown is well preserved and exhibits functional wear over the entire occlusal surface (stage 3; Table 1) and two larges interproximal contact facets. This individual was likely a young adult.

The three rooted molars present preserved mesial roots (16.06 mm) and cementum outgrowth between the distal roots. The pulp cavity extends until the mesial and distal roots diverge (SOM Fig. S4). Additionally, a small enamel extension connects to the buccal inter-radicular groove (grade 1; SOM Table S5b). The crown has a trapezoid outline, with well-defined mesial cusps and a Hyp nearly as developed as the Met (Pro > Pa > Met > Hyp; SOM Table S5b). The narrow sagittal sulcus separates the Pro from the Met until the crista obliqua (grade 2; SOM Table S5b). Deep sulci are visible perpendicular to the latter, isolating the Hyp and Pa.

At the EDJ, the marginal ridge is not continuous and flattens at the Pro distal accessory ridge, expressed with a more developed ridge on the lingual side of the crown than in the occlusal basin. The crista obliqua is expressed by the Pro distal ridge and flattens at the Met (grade 0; SOM Table S5b). Mesially, a tubercular expression separates the Pro and Pa and aligns with tuberosities on the marginal ridge. The Pa is complex with an accessory mesial ridge joining the mesial marginal ridge, and a low essential crest and distal ridge. However, a large accessory ridge is expressed distally from the Pa, whereas only an accessory dentine horn is expressed distally from the Met.

Right $M^{2/3}$ germ #13 The tooth germ has undergone some acidic degradation (Table 1; Fig. 8; Tillier et al., 2013a), similar to #19, #14, and #5, and presents numerous taphonomic scratches on the buccal crown wall. Less than 2 mm of root development is visible. Thus, this individual probably died during adolescence (minimum of 9.5–11.5 years; maximum of 15.5–16.5 years).

The Pa and Pro are the more developed cusps (Pa ≥ Pro > Met > Hyp; SOM Table S5b), expressed with high distal accessory ridges. Wrinkles are visible on the ridges of the mesial cusps and Met. The Pa's essential crest connects with a central accessory ridge, one of the five present on the mesial marginal ridge. The Pro and Met are separated by a narrow groove at the sagittal sulcus. A distal fovea is present between the Hyp and a distal accessory cusp, and there is a deep intercuspal grooving on the lingual wall. The Met bifurcations join the sagittal sulcus, and the Pro distal hook-like accessory ridge borders it. The reduced Met and Hyp, as well as the small dimensions of the crown, could correspond to a third molar, but the mesiodistal diameter of the crown and EDJ morphology especially lead us to favor an attribution to a second molar for this tooth.

At the EDJ, we can observe rather high horn tips. The Pa and Met have distal accessory dentine horns, whereas the mesial ridges and the tubercular thickening of the marginal ridge distally do not. The crista obliqua, formed with the Met essential crest and the Pro distal accessory ridge, is discontinuous. Nonetheless, a distinct distal fovea is marked distally from the crista obliqua and isolates the Hyp (better expressed at the EDJ than OES). The Hyp mesial crest connects with the Pro distal ridge, forming an angular marginal ridge that flattens toward the dentine horn. Buccally, the Hyp mesial basin joins the cuspal concavity of the Pro.

Right $M^{2/3}$ #28 The tooth is nearly complete, but the roots exhibit taphonomic alterations (Table 1; Fig. 8), with the apices broken (maximal length = 13.35 mm) and manganese inclusion on the cementum. The tooth is not functionally worn, but a mesial

interproximal facet is present. The individual likely lived until adolescence (minimum of 11.5–12.5 years).

There is an overall distal orientation of the tooth's morphological structures, from the crown to the roots. The three roots are nearly completely fused, with a cementum bridge visible between them and an extended pulp cavity (i.e., marked expression of taurodontism; SOM Fig. S4). The crown is large compared to the roots, with strong mesial features (Pro > Pa > Met > Hyp; SOM Table S5b). Furthermore, the Hyp is in a mesial position compared to the Met, which, together with the fusion and distal orientation of the root, raises doubts on the position of this molar. The Pa and Pro are expressed with tubercular distal accessory ridges, especially the postparacone tubercule, whereas those of the Met and Hyp are reduced. The Pa essential crest is bifurcated, with two thick ridges running parallel to the mesial marginal one. The Pro bifurcation connects mesially with a thin accessory ridge to the marginal ridge. The crista obliqua is nearly uninterrupted, with a narrowing of the central sulcus, and borders a distal sulcus or fovea. An anterior fovea is formed with the Pa and mesial marginal ridge groove but lacks a distal border (grade 1; SOM Table S5b), creating a Y-shaped groove with the sagittal sulcus. Additionally, there are accessory cusps located between the Pa and the Met, as well as between the Met and the Hyp.

At the EDJ, the marginal ridge forms asymmetries, curving mesially toward the buccal side and distally toward the lingual side. Each of the lingual cusps has an accessory dentine horn but without significant ridging. The marginal ridge flattens below the Hyp dentine horn. The crista obliqua is continuous (grade 2; SOM Table S5b) and creates a wide distal basin isolating the Hyp. The occlusal basin is more complex mesially from the crista obliqua. Both the Pa and Pro are connected by ridges extending from the mesial marginal ridge, with the Pro ridge forming a mesial bifurcation from its essential crest. Overall, the crown morphology and mesiodistal diameter seem to better fit the M^2 morphology, even if an attribution to M^3 cannot be fully discarded.

Left $M^{2/3}$ #32 This tooth is partially preserved (Table 1; Fig. 8), except for a broken lingual portion of the Hyp; taphonomic effects and striations are also present on the roots. The roots display almost complete apical development (root length = 13.59 mm), without major taphonomic breakage. The tooth occlusal surface is not worn, and only a small mesial interproximal facet is present. This individual likely died during their adolescence (11.5–12.5 years).

The tooth structures are oriented backward. The three roots are partially fused until the apical third of the roots, and the pulp cavity extends to that point (marked taurodontism; SOM Fig. S4), similar to M^3s. However, the crown morphology is more similar to M^2s. The Pro, Pa, and Met exhibit strong ridging (Pro > Pa > Met; SOM Table S5b). The Pa displays a well-defined postparacone tubercule. The Pa essential crest is bifurcated, with the distal ridge joining a thin accessory ridge of the mesial marginal ridge. The mesial bifurcated ridge is parallel to the mesial marginal ridge, forming a small anterior fovea (grade 1; SOM Table S5b). The Met is expressed with fused large ridges, with the distal one wrinkling distally and forming a tubercle at the central sulcus. The crista obliqua is interrupted by a narrow groove at the sagittal sulcus. Accessory cusps are present between the Hyp and Met.

At the EDJ, the crista obliqua is continuous (grade 2; SOM Table S5b). The mesial marginal ridge extends toward the lingual side. Each of the lingual cusps possesses an accessory dentine horn and the distal accessory tubercle. The occlusal basin exhibits greater complexity toward the mesial aspect of the continuous crista obliqua, especially with the mesial cusps and accessory ridging on the mesial marginal ridge. One of these ridges connects to the Pa and Pro essential crest at the sagittal sulcus.

Left M^3 #5 The tooth, while complete (Table 1; Fig. 8; David et al., 2009; Tillier et al., 2013a), exhibits sign of enzymatic alterations from partial digestion (glossy external aspect, eroded cervix, and opened root apices). The cusps are worn (stage 4; Table 1), and only the sulci are preserved to appreciate the occlusal morphology. Furthermore, only a mesial interproximal facet is present. This individual died as a middle-aged adult.

The tooth features three separated roots (maximal length = 13.19 mm), with the buccal roots fused and a hook-like root lingually. The roots are oriented distally relative to the cervix. The pulp cavity is slightly extended (SOM Fig. S4). The crown outline appears constrained mesiodistally, with a reduced Met and Hyp. The four main cusps are present (Pro > Pa > Met > Hyp), with accessory expressions between the Hyp and Met and between the Pa and Met. Accessory ridges are also expressed mesially. A 'Y-shaped' fovea is dissociated from the sagittal sulcus mesially.

At the EDJ, an anterior fovea is expressed mesially from the Pa (grade 1; SOM Table S5b), isolated from the mesial complexity by a thin ridge that joins the trifurcated essential crest of the Pa. A Pa accessory ridge is expressed distally, although lacking a distinctly expressed accessory dentine horn compared to the Pro and Met. The distal accessory cusp is clearly defined at the EDJ. The crista obliqua is not expressed (grade 0; SOM Table S5b). On the lingual tooth wall, a small tubercle is absent from the OES but present on the EDJ (white arrow, Fig. 8) and aligned with the Pro distal accessory ridge. Mesially, a ridge is also present and supposedly extends into the cusp apex.

Figure 9. Lower permanent canines from the Grotte du Bison: RC_1 #8; RC_1 #23 (Table 1); with the OES and the EDJ in occlusal, distal, labial, and lingual views (every view in SOM Fig. S2b). The arrows indicate distal accessory dentine horn (#8) and ridge (#23). The asterisks indicate linear hypoplasic events. Scale bar = 5 mm. EDJ = enamel–dentine junction; OES = occlusal enamel surface.

Right M^3 germ #34 This tooth germ appears weathered (taphonomically discolored areas), and the cervix is broken (Table 1; Fig. 8). Despite the crown breakage, the upper part of the pulp chamber is preserved (white arrow, Fig. 8). However, the tooth does not have any occlusal wear and was likely unerupted. Thus, this individual died in their adolescence (ca. 14.5–15.5 years).

The crown features three primary sections or cusps and well-developed ridges mesially (Met > Pa > Pro = Hyp), as the sagittal sulcus forms a distinct 'X shape.' The mesial accessory ridges create a noticeable tubercle at the central sulcus. The Pa exhibits a large distal accessory ridge, whereas the Met is centered in the distal portion of the tooth. The Pro mirrors the Pa, and the Hyp does so with the Pa distal accessory ridge. A high degree of Carabelli's trait expression is discernible on the lingual side (grade 6; SOM Table S5b).

At the EDJ, the mesial complexities and the Pa distal ridge are expressed with accessory dentine horns. The essential crests of the buccal cusps are well expressed, contrary to the lingual ones. Two ridges connect the Hyp to the Pro, a marginal ridge (translated into a Carabelli's expression at the OES) and an accessory ridge oriented mesiodistally.

Right C_1 #8 The tooth is complete and well preserved (Table 1; Fig. 9), but a large frontal fracture runs through the tooth and gradually tapers toward the root apex. Residual calculus deposits are present around the crown, above the gingival margin, with the most significant accumulation observed mesiobuccally. On the buccal surface, perikymata are easily discernible, with some taphonomically colored (visible on the buccal view). Some hypercementosis developed on the root apex, over a quarter of the root length and extending within the mesiodistal radicular grooves of the root, which is shaped like an '8' (5.4 mm of hypercementosis over 16.18 mm of root). The crown displays substantial occlusal wear (stage 4; Table 1) and is characterized by two main wear surfaces: a horizontally oriented mesial surface and a concave, obliquely oriented distal surface (mesiodistally). Additionally, the labial structures of the crown are polished, and a significant interproximal contact facet is present on the distal side. It is likely that this tooth belonged to an individual deceased during their early adulthood.

Both the crown and root profiles exhibit pronounced convexities. Thus, the tooth is cyrtodont overall. On the crown, the distal ridge is visible and protrudes distally, although it is narrowed by the interproximal wear facet. The mesial ridge is smoothed but can still be identified, especially due to the occlusal wear, where the EDJ forms a distinct 'beading' appearance.

On the EDJ, the crown is slightly shoveled (grade 5; SOM Table S3), with the marginal ridges converging at the slightly elevated cingulum. Near the wear surface, a developed central ridge is discernible. Additionally, there is a clear distal tuberculum on the prominent distal marginal ridge.

Right C_1 #23 This tooth is almost complete (Table 1; Fig. 9), with enamel breakage of the distal marginal ridge and fractured root apex (root length = 15.98 mm). The enamel surface appears dull, and small taphonomic pitting is visible on the root. Two wide linear hypoplasia lines (>1 mm each) create depressions labially. The crown apex is functionally worn (stage 2; Table 1) and mesial and distal interproximal facets are present. This individual passed away during adolescence (ca. 11.5–12.5 years).

The tooth profile is cyrtodont, with a marked convex shape. The crown displays a moderate shoveling (grade 3; SOM Table S3) characterized by a deep central sulcus and prominent marginal ridges that fade as they approach the cingulum. The mesial marginal ridge thickens before reaching the cingulum, with a groove separating the two. The distal ridge is broken, but its presence can only be inferred from the thickness of the fracture. While the cingulum is not markedly pronounced, there are numerous tubercular thickenings along the incisal edge on the lingual side.

In addition to these subtle tubercular features on the marginal ridges at the OES, a faint distal accessory ridge can be observed (Fig. 3). The latter is expressed at the EDJ by an accessory dentine horn. However, a slight ridging appears on the labial side. At the EDJ, the central ridge is not distinctly expressed, but the marginal dentine ridges are well defined and oriented inward. The cingulum is marked mesially by a small 'dentine-horn-like' protrusion of the continuous marginal ridge.

Right P_3 #9 The tooth, although complete (Table 1; Fig. 10), is frontally broken, with the fracture visible in the middle when seen in distal view. Calculus patches are visible on both the buccal and lingual sides. The occlusal wear (stage 3; Table 1) is characterized by a mesial facet that extends toward the buccal side and an oblique facet dipping distally. While the lingual structures appear smoothed, they lack any distinct faceting. Both the mesial and buccal sides show significant interproximal contact facets. It is likely that this individual was a young to middle-aged adult at death.

The buccal profile of the tooth is convex and can be considered cyrtodont despite the worn Pro. The root is relatively short (15.2 mm) and superinferiorly concave distally. The mesial side of the root features subvertical furrows and a central protrusion. The crown appears elongated in the buccolingual direction. The essential crest remains continuous (grade 2; SOM Table S4), marked by deep mesial and buccal sulci on the lingual side. The apex of the Met is worn, and the marginal ridge shows a distolingual asymmetry (grade 1; SOM Table S4) and protruding distal marginal ridge (multiple lingual cusps; grade 2; SOM Table S4).

At the EDJ, the marginal ridges and transverse crest are continuous (grades 2 and 1; SOM Table S4), with the presence of a distolingual extension of the Met marginal ridge.

Left P_3 germ #24 This tooth germ is taphonomically colored (ocher) and discolored (Table 1; Fig. 10). The crown is complete with a beginning of root development (visible in distal view), suggesting that this individual died in early childhood (5.5–6.5 years).

The crown, viewed from the occlusal surface, takes on a rhomboidal shape with rounded mesiolingual and buccodistal contours (contour asymmetry; grade 0; SOM Table S4). A shallow anterior fovea is present, bordered mesially by the mesial marginal ridge of the Pro and distally by the essential crest of the Met (transverse crest; grade 0; SOM Table S4) and by the mesial bifurcation of the Pro, as both structures are separated by a deep, continuous sagittal sulcus. The seemingly bifurcated essential crest of the Pro is higher distally but is overall less expressed than the pronounced distal accessory ridge (grade 3; SOM Table S4). The Pro distal bifurcation and distal accessory ridge align with a slight tuberculum (grade 2; SOM Table S4) on the Met, distally adjacent to the essential crest as they are separated from each other by a deep sulcus.

At the EDJ, the Pro distal accessory ridge and the Met essential crest are visible (grade 2; SOM Table S4). A faint trace of the Pro essential crest is noticeable near the sagittal sulcus. The marginal ridge, after a marked mesial expression, is interrupted before reaching the tip of the Met (grade 1a; SOM Table S4). Finally, on the mesial edge of the buccal face, there is a noticeable groove (see white arrow, Fig. 10).

Left P_3 #26 The tooth is damaged (Table 1; Fig. 10), with most of the root missing (7.01 mm preserved mesially). Over the distal half of the tooth, the cervical area of the crown is broken and the root eroded. The overall surface of the tooth is slightly weathered and shows some manganese patches. There is a slight occlusal wear

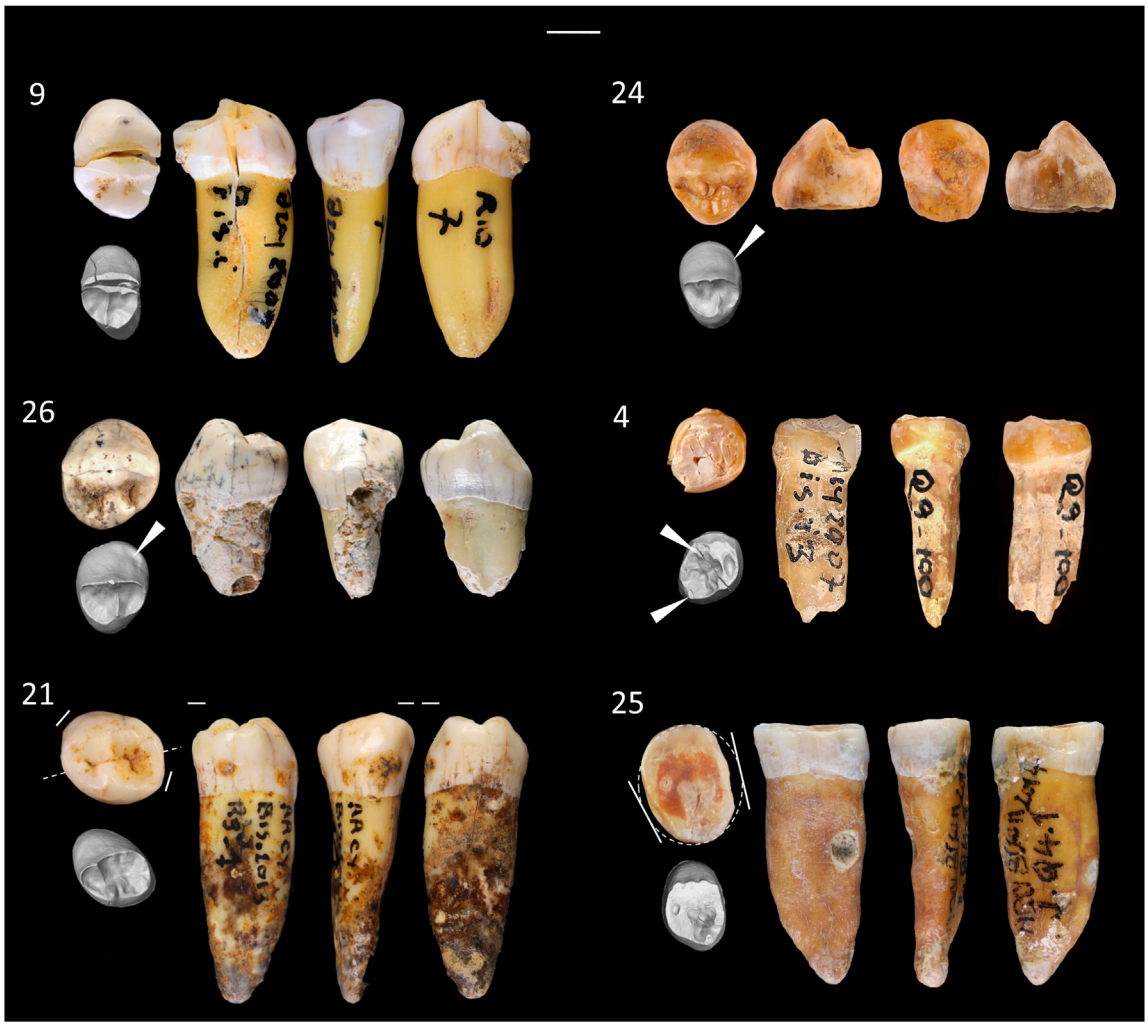

Figure 10. Lower premolars from the Grotte du Bison: RP_3 #9; LP_3 germ #24; LP_3 #26; LP_4 #4; RP_4 #21; RP_4 #25 (Table 1); with the OES and the EDJ in occlusal, distal, buccal, and mesial views (every view in SOM Fig. S2c). The arrows indicate the distal accessory ridge and cusp of #4. On the teeth #21 and #25, the white line highlights the mesial and distal interproximal contact facets at the occlusal view; with for #21 the distal one on the distal view, and the mesial one on the buccal and mesial views. Additionally, a dashed line indicates the estimated crown contour of the tooth #25. Scale bar = 5 mm. EDJ = enamel–dentine junction; OES = occlusal enamel surface.

(stage 3; Table 1) characterized by oblique buccal and mesial facets, and two interproximal contact facets. This individual seems to be a young adolescent (ca. 12.5 years).

The remaining root surface mesially shows the beginning of a shallow subvertical groove. The crown has a rounded outline, with a beveled and mesially placed Met (grade 1; SOM Table S4) and convex buccal linguodistal faces (crown asymmetry; grade 2; SOM Table S4). The transverse crest is interrupted by a shallow groove (grade 1; SOM Table S4), whereas a deep anterior fovea is expressed mesially. Both the lingual and buccal structures are large but without any noticeable tubercle expression (grade 2; SOM Table S4).

At the EDJ, the buccal side of the Pro presents a pronounced mesial groove (see white arrow, Fig. 10; stage 1; SOM Table S4). The continuous marginal ridge is straight buccally, but lingually, two lobes are formed by their high convexity (grade 2; SOM Table S4), with a complex distal basin. The transverse crest connects to the Pro but flattens to the occlusal basin (grade 2; SOM Table S4), and a small protuberance marks the distal accessory ridge on the Pro (grade 1; SOM Table S4).

Left P_4 #4 The tooth is heavily damaged (Table 1; Fig. 10), exhibiting alterations associated with carnivore partial digestion and taphonomic erosion, especially on the mesial and buccal side. Thus, the root surface is brittle, and a substantial part of the root apex is broken (12.40 mm preserved distally) along with a distolingual portion of enamel. Nearly a third of the crown's height is functionally worn (stage 4; Table 1). This individual could have died as a middle-aged adult.

While discernible sulci along the occlusal surface provide insights into the intricacies of the OES, the EDJ provides a more comprehensive view of the crown's morphology. At the EDJ, a well-defined anterior fovea is apparent, enclosed distally by a small ridge connecting to the worn dentine horns of the main cusps. Distally, a wide and complex basin and an isolated lingual accessory cusp contribute to the pronounced asymmetry of the crown (grade 1; SOM Table S4). Furthermore, additional accessory structures are visible, including a distal lateral accessory ridge, remnants of the bifurcated ridge of the Met, and distal tubercles aligned sagittally with the anterior fovea.

Right P_4 #21 The tooth is complete and well preserved (Table 1; Fig. 10), with few traces of taphonomic erosion and manganese coloration on the root. Patches of calculus surround the crown, especially on the buccal and distal sides. Little hypercementosis is developed on the root apex (root length = 17.5 mm). There is

minimal occlusal wear, primarily manifesting as oblique facets on the mesial structures (stage 2; Table 1), and clear interproximal facets are seen mesiobuccally and distolingually. This individual probably died during their adolescence (ca. 12.5–14.5 years).

The tooth exhibits a slightly convex buccal profile and is considered cyrtodont. The crown morphology, root structures, and the interproximal contact facets are not aligned. The interproximal contact facets are neither aligned with the sagittal sulcus nor with the mesial and distal parts of the roots. The morphological structures on the occlusal surface are rotated compared to the crown and root walls; with a mesiolingual to buccodistal diversion of the sagittal sulcus and adjacent features. Similar tooth crown rotation is described by Rougier et al. (2013) on Krapina P_3s. The Pro is in mesial position while the Met seems central (grade 0; SOM Table S4), with the respective distal tuberosities in a buccal and distal disposition. The interproximal facets are positioned on the mesiobuccal part of the Pro and distolingual portion of the lingual accessory cusp (as indicated in Fig. 10 by the interproximal contact facets outlined relative to the crown morphology and sagittal sulcus). Thus, the crown is highly asymmetric (grade 1; SOM Table S4). This asymmetry is especially heightened with the developed expression of accessory structures. The marginal ridges are well developed with tubercular expressions mesially and two accessory cusps distally. Additionally, the two distal accessory ridges of the Pro form apically a cusp-like protuberance, expressed with a protuberance buccally. The essential crests are large, and the Met is distally bifurcated. All the structures are well separated by the continuous central sulcus (transverse crest; grade 1a; SOM Table S4) and deep lateral sulci.

At the EDJ, the marginal ridge is nearly continuous, with a distal step adjacent to the lingual dentine horn (grade 1b; SOM Table S4). Numerous accessory dentine horns are present over the marginal ridge. The two distal accessory ridges (grade 3; SOM Table S4) on the Pro present dentine horns at the marginal ridge. The Met presents two distal accessory ridges: a tubercle-like one aligned with the bifurcated essential crest and a smaller one. The transverse crest is interrupted by the central sulcus (grade 0; SOM Table S4). Finally, a distolingual and a distobuccal accessory cusp are well defined.

Right P_4 #25 Taphonomic damage is present on the root, notably circular effects mesiolingually and distobuccally (Table 1; Fig. 10). The crown is well preserved, but a flake of cement is missing from the root apex, reducing the root height (17.4 mm). A substantial buccal calculus deposit is present on the mesiolingual quarter of the crown, likely extending below the gingival margin. The extensive

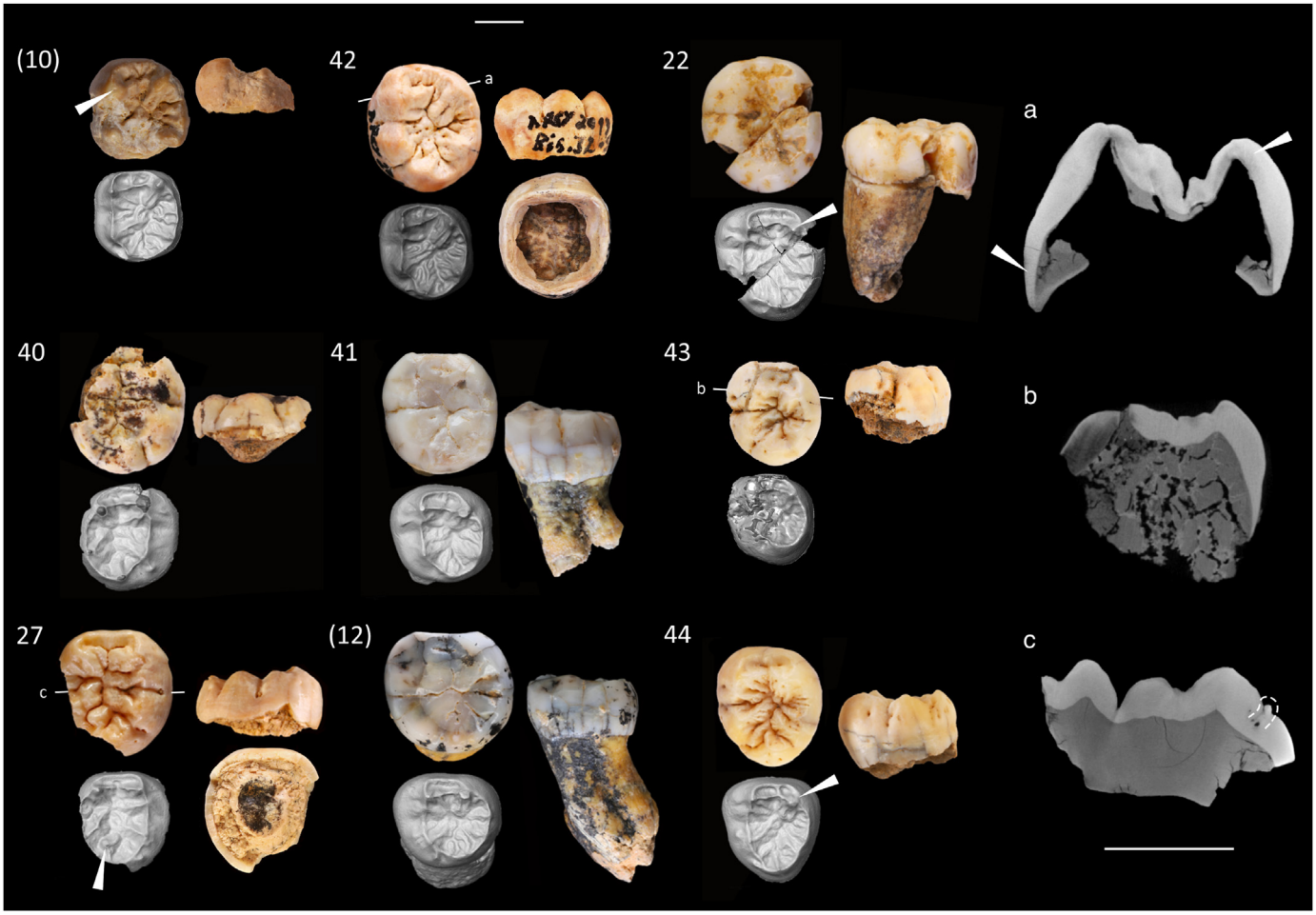

Figure 11. Lower permanent molars from the Grotte du Bison: LM_1 germ #10; LM_1 germ #42; $LM_{2/1}$ #22; RM_2 #40; LM_2 #41; LM_2 germ #43; $RM_{2/3}$ #27; LM_3 #12; LM_3 #44 (Table 1); with the OES and the EDJ in occlusal and distal views (every view in SOM Fig. S2e). On #22 and #44, the arrow indicates the Met dentine horn shift toward the center of the occlusion. Arrows on the mesial developmental slice (a) of #42 indicates visible enamel structure in areas of enamel demineralization. The developmental slice of #43 (b) shows the enamel thickness of the tooth. For #27, (c) a dashed shape highlights a small enamel node the groove between the C7 and Ent (on a slice interpolated distally from the mesial developmental slice). The parentheses show the previously published tooth. Scale bar = 5 mm. EDJ = enamel–dentine junction; OES = occlusal enamel surfacebelcast.

occlusal wear has reduced the prominent crown structures (stage 4; Table 1). The interproximal contact facets have also significantly altered the crown outline (Fig. 5). The individual was likely middle-aged or elderly.

The buccal profile of the tooth has a slightly corrugated morphology, whereas the root presents a convex profile on the lingual side. On the mesial side, a subvertical protrusion is present, bordered by a wide groove buccally and a marked one lingually. Despite the considerable dentine exposure in the occlusal area, the main structures remain visible. The lingual cusp is mesially placed (grade 1; SOM Table S4), and distinct distal and mesial sulci are present and perpendicular to the sagittal sulcus. These sulci likely indicate the expression of the anterior fovea and the significant development of distal accessory features, particularly the second lingual cusp (grade 2; SOM Table S4).

The identification of this tooth relies primarily on the EDJ and the pulp morphology (Fig. 5; SOM Fig. 4), including the presence of a complex distal basin and accessory cusp expression, the mesial positioning of the Met (grade 1; SOM Table S4), and the presence of multiple pulp horns.

Left M_1 germ #10 The tooth displays considerable taphonomic degradation, with its distobuccal half almost entirely eroded (Table 1; Fig. 11; Tillier et al., 2013a). The crown is not fully developed and, being nonfunctional, shows apical pits probably formed through ameloblast resorption and proteolysis during the maturation process of the enamel, or from the inner enamel epithelium morphology (especially on the Pro; white arrow, Fig. 11; Smith, 1979; Henrion et al., 2023). The individual likely died during early childhood (2.5–3.5 years).

The tooth presents intricate occlusal ridging, featuring double ridges on the Met, Ent, and C7. The central ridge of the Pro forms the distal border of the anterior fovea (grade 3; SOM Table S5b), whereas a distal bifurcation of this ridge connects with the sagittal sulcus at the junction of the Met and Hyp.

At the EDJ, the entire occlusal morphology is well preserved, and the pronounced ridging closely resembles the OES. A C6 is present, and the Hyp bifurcation is centrally located within the occlusal basin, appearing as an accessory cusp. The anterior fovea is interrupted by an accessory ridge in the middle of the mesial marginal ridge (grade 3; SOM Table S5b). On the lingual side, each cusp and accessory ridge has a well-expressed dentine horn at the marginal ridge. However, the Met has an occlusally displaced dentine horn, dissociated from the marginal ridge. On the buccal side, the dentine horns of the distal accessory ridges are not as clearly defined. Finally, an accessory ridge is observed on the distobuccal border, opposite to the Pro distal accessory ridge.

Left M_1 germ #42 This germ is very well preserved, with only minor subvertical cracks (Table 1; Fig. 11). The cervical area does not seem eroded even though a slight weathering of the tooth is suspected by its coloration and dull surface. These stigmata suggest a singular taphonomic effect on immature enamel supported by the density of the overall enamel cap, in addition to the chemical erosion stigmata on the horn tips and sulci (superficial demineralized areas; Fig. 11a). Furthermore, the dentine is mostly gone from the germ, leaving some patches in the cusp apices and on the cervix. The latter suggests that the pulp cavity was not developed. On the mesial marginal ridge, a deep circular depression is present, interpreted as a developmental feature rather than a pitted hypoplasia. However, pitted hypoplasia might be scattered within the occlusal furrows and exacerbated by taphonomic processes (desiccation and trampling). This individual likely died during childhood (ca. 2.5 years).

The crown is oval, with bulbous cusps. The central ridge of the Pro is larger than the ridges on the other cusps (Pro > Met > Hyp ≥ C5 > Ent). The Met has two well-expressed ridges, with centrally positioned essential crest and distal ridge. The Hyp, however, presents an important central bifurcation. The C5 and Ent are complex, with a wrinkled mesial ridge, but the Ent seems trifurcated, and the C5 ridges form a cusp-like tubercle at the sagittal sulcus. The C6 and C7 are similarly expressed. The anterior fovea is distally bordered by the Pro essential crest (grade 2; SOM Table S5b), displaying a cusp-like expression. The mesial marginal ridge is complex, featuring accessory ridges between the Pro and Met, similar to the Met mesial accessory ridge.

The EDJ is reconstructed based on the negative expression on the inside of the enamel cap. The heavy ridging in the occlusal bassin corresponds to the OES complexity. At the EDJ, the marginal ridge presents intercuspal convexities and a rounded lingual contour. Accessory dentine horns are present mesially from the Pro, in the center of the mesial marginal ridge, and subtly above the Met mesial accessory ridge. The lingual dentine horns are directed inward, toward the occlusal basin. The anterior fovea is triangular (mid-trigonid crest origin; grade 1; SOM Table S5b) and distally bordered only by the Pro essential crest and its tubercular extension that flattens into the mesial marginal ridge lingually.

Left $M_{2/1}$ #22 The tooth is poorly preserved and shows extensive taphonomic damage (Table 1; Fig. 11). The crown is fractured obliquely and missing the distal portions of the Hyp and Met. The crown and roots are separated with a cervical area eroded mesially that hinders our understanding of the initial positioning of the roots. Only the mesial parts of the roots are preserved (maximal length = 13.8 mm), in two eroded fragments. Slight hypercementosis is also visible. Only a mesial interproximal facet is present, and the occlusal surface exhibits slight functional wear (stage 2; Table 1). It is likely that this individual died during their adolescence (12.5–14.5 years).

The mesial roots can be reconstructed in a subvertical position considering the mesial fracture and the preserved cervix distally. Specifically, the root apex is not oriented distally, a feature that is uncommon and primarily observed in M_1s. The roots could be highly taurodont considering the wide opening drawn distally by the fractured root, showing the pulp cavity. The crown has an oval outline, and its five main cusps are roughly proportional in size (Pro > Hyp ≥ Met ≥ Ent ≥ C5). The C6 and C7 are both present and well developed. Although the C7 is heavily damaged, it can still be identified. However, the complexity of C5 cannot be discerned due to taphonomic alterations. Each cusp displays intricate structures with deep lateral grooves. The Pro lateral accessory ridges are more pronounced than the central one. The Met also appears to have two lateral accessory ridges and a bifurcated central one. The Hyp and Ent have large and shallow lateral grooves around the central ridge. The C6 exhibits a small distal accessory ridge. The anterior fovea is deep, featuring a central tubercle on the mesial marginal ridge (grade 3; SOM Table S5b). However, the distal border of the fovea is interrupted (mid-trigonid crest; grade 1; SOM Table S5b) by a slight intercuspal groove situated between the mesial ridges on the Pro and Met. The protostylid is well developed and is accompanied by a buccal accessory cuspule on the Hyp (grade 5; SOM Table S5b).

At the EDJ, the crown shape is more squared mesially and becomes triangular toward the distal portion. The marginal ridge is convex lingually and angular buccally and slightly narrows distally. Overall, the crown morphology, especially at the EDJ, fits the M_2s. The main cusps exhibit a high occlusal complexity but with low ridges. The Met position is shifted into the occlusal basin. Accessory dentine horns are present on the essential crest of the Met and mesial ridge of the Pro. A distal accessory ridge is expressed on the Pro, without a dentine horn. The expression of the Ent is similar but reduced. The Met horn tip (Fig. 6) is distanced from the lateral ridge and appears to have a complex ridging distally from the essential

crest. The C5 is expressed with an accessory dentine horn, higher than the C6 dentine horn. The anterior fovea exhibits a continuous distal border that flattens at the Pro (mid-trigonid crest; grade 3; SOM Table S5b). The mesial marginal ridge displays some tubercular expressions. The buccal side of the crown is highly complex, with deep sulci, and both the Pro and Hyp feature tubercles aligned with the main dentine horns, with accessory ridges surrounding the intercuspal groove, associated with the protostylid expression at the OES. The crown also presents an accessory distobuccal cuspule.

Right M_2 #40 The tooth is poorly preserved (Table 1; Fig. 11), with only the occlusal half of the crown remaining and mesial and lingual breaks (from the mesial part of the Met to the middle of the Ent). Manganese patches are widespread on the occlusal surface, and numerous cracks surround the crown. Occlusal wear is moderate, with minor dentine exposure on the cusp tips (stage 2; Table 1). No distal interproximal facet is discernible. This individual could have died in their adolescence (11.5–16.0 years).

The crown exhibits a rounded outline and features prominent ridges on the Pro and Met, as well as intricate ridging on the Hyp and Ent. The C5 is markedly expressed (Pro > Hyp > C5). There is a probable expression of C6 and C7 between the Hyp and C5, and between the Met and entoconulid, with a likely wrinkle mesially. The anterior fovea is pronounced with the distal ridge interrupted by the sagittal sulcus (grade 3; SOM Table S5b). The protostylid is expressed by a grooving on the Pro (grade 1; SOM Table S5b). Furthermore, the Hyp buccal wall presents a tuberosity distally.

At the EDJ, the marginal ridge is angular on the buccal side and rounded on the lingual side. The C6 and C7 are identified by intercuspal tuberosities, with inward projections of the marginal ridge. The dentine horns of the Met and Ent are positioned away from the marginal ridge. The Ent displays more pronounced ridging, especially mesially. The well-expressed mesial accessory ridge on the Met joins the Pro ridge continuously, forming uninterrupted fovea borders (grade 3; SOM Table S5b). The Pro is expressed with marked ridges, with the mesial ridge featuring a cusp-like tubercle toward the sagittal sulcus, and a bifurcated distal ridge. On the buccal wall, the protostylid is expressed by a small ridging, and a tubercle extends from the Hyp distal accessory ridge at the occlusal surface.

Left M_2 #41 This tooth is partially preserved (Table 1; Fig. 11). The crown is complete, but nearly half of the roots are taphonomically broken (maximal root length = 4 mm distally, 10.4 mm mesially). The remaining cementum or dentine is flaky. Small calculus patches remain buccally and lingually. The occlusal wear is mild, featuring dentine patches on the mesial cusps (stage 2; Table 1) and large oblique facets mesially. Furthermore, two large interproximal facets are present. This individual likely died in early adulthood.

The molar has two pairs of roots distally divergent, with dissociated mesial ones and minor pulp extension to this point (SOM Fig. S4). The crown outline is square to rounded, with four well-developed main cusps and a small C5 (Pro > Met > Hyp > Ent > C5). The structures are well separated, and a narrow anterior fovea is present. The C6 and C7 are noticeable due to the central furrows separating the cusps, with a small furrow separating the C6 from the thinner C5, a distal nook separating the C7 from the Met, and lateral grooves in the crown wall drawing it apart from the main lingual cusps. An enamel extension is seen on the buccal side and the protostylid slightly expressed.

At the EDJ, the marginal ridge has an angular buccal aspect, and the lingual side is rounded. The Met is distanced from the marginal ridge, whereas the Ent horn is directed toward the occlusal basin. The mesial ridges of the Ent and Hyp are distinctly expressed and isolated. There is a slight expression of C7. The distal accessory ridge of the Pro (also forming a high buccal wall ridge) is expressed as a cusp-like tuberosity. The fovea is large, with an uninterrupted distal border formed by the Pro and Met mesial ridges (grade 3; SOM Table S5b) and a central tubercle on the mesial marginal ridge.

Left M_2 #43 The tooth crown is fractured both mesially and buccally (Table 1; Fig. 11). The roots were also taphonomically broken, with the cervical enamel missing buccally. A pronounced hypoplasic pitting is observed not only on the buccal side of the crown but also on the occlusal surface. A well-defined mesial interproximal contact facet is present as well as occlusal wear on the Pro apex (stage 2; Table 1). The individual likely died during adolescence (11.5–16.5 years).

Despite the breakage of the crown, the occlusal contour appears rounded and small. However, the enamel appears as thick as observed on other permanent molars (Fig. 11b). The occlusal morphology is complex with deep sulci isolating the accessory ridging and the five main cusps (Pro > Met > Ent > Hyp > C5). A C7 is faintly expressed but is well isolated from the distal cusps with a deep transverse sulcus in the continuation of the Pro and Met intercuspal grooves. Those mesial cusps are merged mesially to form a thick distal border to the anterior fovea. This fovea is interrupted by a transverse ridge from the mesial marginal ridge.

The marginal ridge at the EDJ reveals the asymmetry of the crown toward the distolingual side. The ridge conformation at the OES is reflected identically at the EDJ but with a lower elevation. Deep and wide intercuspal grooves are expressed on the buccal wall, without marginal ridge between the Pro and Hyp (visible despite the poor buccomesial preservation of the EDJ).

Right $M_{3/2}$ germ #27 This germ is broken lingually from the Met to the C5 apices, as well as the cervix (Table 1; Fig. 11). Pitted hypoplasia is present on the preserved buccal wall, with shallower pits mesially from the Pro and on the C5 than in both intercuspal grooves of the Hyp. The tooth is unworn (stage 1; Table 1), without interproximal contact facet. However, the pulp cavity had started to develop. This individual was likely an adolescent when they died (ca. 14.5–15.5 years).

The remaining crown outline is rounded. All the essential crests of the cusps appear to end with a tubercular expression at the central sulcus. The Pro distal marginal ridge is expressed as an accessory cusp. Buccally, an enamel protuberance is seen at the base of the intercuspal groove between the Pro and Hyp (Fig. 11c). The Met and Pro essential crest are highly complex and separated by the sagittal sulcus, forming an interrupted distal border for the narrow anterior fovea (grade 2; SOM Table S5b). A tubercular expression is observed in the fovea from the center of the marginal ridge.

At the EDJ, the marginal ridge maintains a rounded shape, distally from the Met and Pro dentine horns, positioned inward from the marginal ridge. However, the mesial marginal ridge forms a rectangular notch, isolated from the surrounding marginal ridging. The mesial ridges of the Met and Pro do not connect to close the anterior fovea distal ridge (grade 1; SOM Table S5b), and a tuberosity is expressed in the center of the groove. However, the Pro is less complex, although featuring deep lateral grooves around the horn tip. The essential crests of the Hyp, C5, and Ent exhibit similar complexity. The C6 accessory cusp ridge is robust and forms a hook mesially and a small accessory dentine horn distally. On the buccal face, thin ridges surround the Hyp horn tip, and a buccal ridge forms a tubercle on the C5.

Left M_3 #12 The tooth is almost complete (Table 1; Fig. 11; Tillier et al., 2013a), with a well-preserved crown and nearly completely preserved roots (maximal length = 14.75 mm). However, the

cementum and root apices are taphonomically degraded, with a remnant of high apical hypercementosis. Except at the apex, there is no clear separation of the roots; hence, we consider the roots almost fused, without taurodontism (SOM Fig. S4). Calculus patches are present on the buccal wall of the crown. The tooth was functional (stage 2; Table 1), and only a wide interproximal facet is present mesially. Thus, this individual was most likely a middle-aged adult.

The occlusal contour of the crown is round. The buccal cusps are large, with a reduced C5 equivalent to the main and accessory lingual cusps (Pro > Hyp > Met > Ent > C6 ≥ C7 > C5).

At the EDJ, the marginal ridge is rounded overall, with the mesial marginal ridge forming a rectangular notch at the anterior fovea (mid-trigonid crest origin; grade 1; SOM Table S5b). Distally, the Pro trifurcated essential crest forms an accessory cusp and joins the mesial trifurcation of the Met essential crest. Both the Pro and Met feature a distal accessory ridge expressed as an accessory cusp, with prominent mesial wrinkling, especially on the Met. The expression of the C7 is more pronounced than that of the Ent. The C5 and C6 are both faintly expressed at the EDJ. The buccal side of the Hyp is ridged mesially, and there is a cusp-like tubercle distally.

Left M_3 #44 The tooth is developed (Table 1; Fig. 11) down to the cervical portion of the root (<4 mm). The root is eroded up to the crown buccally, and few cement deposits remain distolingually. However, the hollow dentine structure within the root and crown suggests that root development had not progressed much beyond the stage evident in the preserved portion. About mid-way up the overall crown height, a linear hypoplasia is visible distally, and numerous pitted hypoplasia irregularly mark the occlusal surface and the distal and buccal crown walls. This individual died during adolescence (ca. 14.5 years).

The crown outline is triangular distally. The main cusps are well-defined (Pro > Met > Ent > Hyp > C5). The lateral ridges of the Pro are highly complex. The mesial accessory ridge exhibits a distal bifurcation of nearly equal thickness to the mesial one. Distally from the distal accessory ridge, additional thin ridges are present. The Met shows a similar pattern, with a trifurcation of the mesial ridge, a deflecting wrinkle on the distal ridge, and numerous thin distal accessory ridges. One of these ridges separates the cusp from the C7. The C7 and C5 exhibit a similar expression with a short mesial accessory ridge. However, the C5 is much larger. The expressions of the Hyp and Ent also feature highly complex central ridges. Additionally, distally, an accessory ridge detaches from the Ent, forming a cusp-like ridge. Three tubercles are expressed on the mesial marginal ridge, with the central one connecting to the marginal ridge of the Met, thus interrupting the deep anterior fovea (grade 3; SOM Table S5b). A protostylid expression is drawn out from the deep intercuspal groove by the pitted hypoplasias on the buccal face of the Hyp (grade 3; SOM Table S5b). The intercuspal sulcus between the Hyp and C5 is also well expressed, featuring a cusp-like protuberance in the center, accentuated by the presence of pitted hypoplasia in the morphological grooving.

At the EDJ, the marginal ridge is convex on the lingual side and straight on the buccal side. The complexity of the distal ridges is not high compared to the overall level of the surrounding occlusal bassin. The mesial ridges of the Pro and Met exhibit a midway thickening. Below the tubercle of the Met, a ridge interrupts the large fovea and joins the distal border of the fovea, marked by the mesial ridges of the Pro and Met (grade 3; SOM Table S5b). Furthermore, the Met dentine horn is shifted away from the marginal ridge (Fig. 6). A deep intercuspal groove is present distally from the buccal ridge that corresponds to the Pro distal accessory ridge at the occlusal basin. A slight tuberosity is also observed on the buccal wall, mesially from the Hyp dentin horn. On the buccal face, accessory tubercles are expressed and marked by a mesial groove, mesially from the Hyp and C5 dentine horn. The latter is continuous with the marginal ridge hook formed between the Hyp distal accessory ridge and C5.

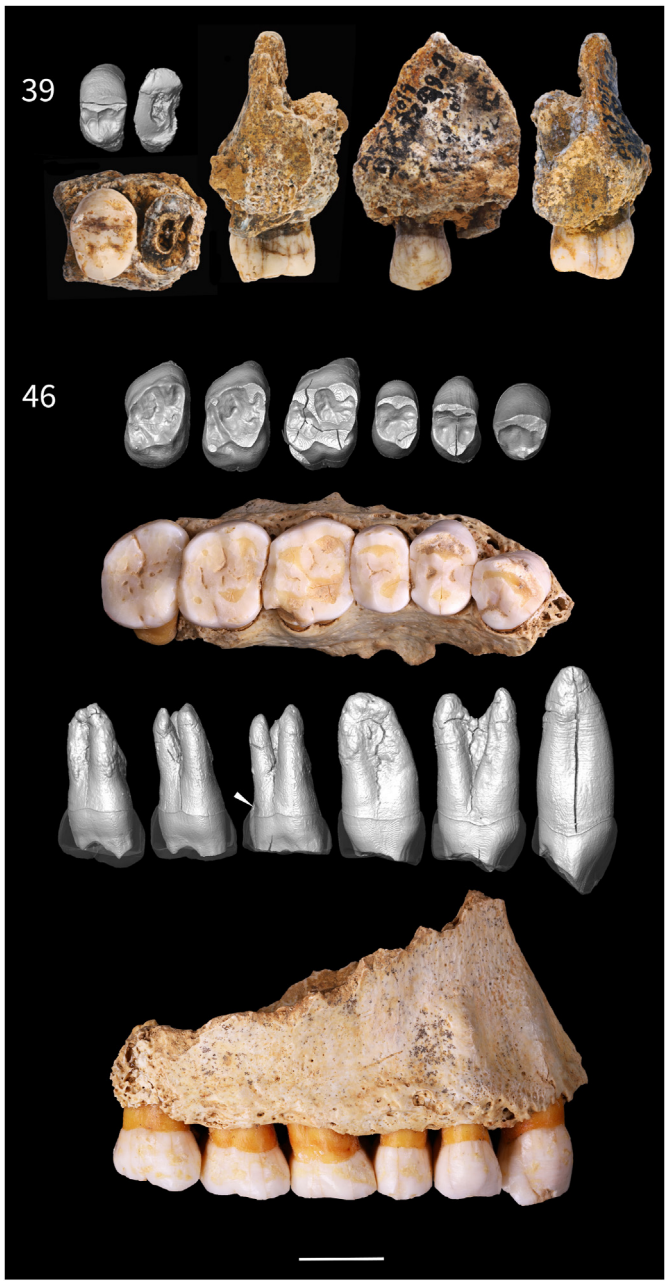

Figure 12. The maxilla fragment #39 (LP^3, and broken LP^4), with the OES and the EDJ in occlusal, distal, buccal, and mesial views (every view in SOM Fig. S2c). The maxilla fragment # 46 (RC^1–RM^3), with photographs in occlusal and buccal views, the digital reconstructions of the dentine surface in occlusal view, and the distal view of the teeth showing the dentine, with transparent enamel cap (every view in SOM Fig. S2f). Scale bars = 1 cm. EDJ = enamel–dentine junction; OES = occlusal enamel surface.

3.4. Teeth in the dental arch

Left maxilla fragment: P^3–P^4 #39 A fragment of maxilla is preserved, large enough to hold two premolars (Table 1; Fig. 12). While the P^3 crown is well preserved, with traces of taphonomic coloration and lingual calculus patches, the P^4 is broken bellow the cervix. Both teeth present hypercementosis on the distal quarter of the roots. The P^3 crown is functionally worn (stage 3; Table 1), with a

considerable subvertical chip (>1 mm; Belcastro et al., 2018) placed distoapically on the buccal side. The maxilla belongs to an individual that died in early adulthood.

Both teeth have bifurcated roots, occurring at approximately two-thirds of their total height. The bifurcation is less marked on the P^4, with a thicker cementum wall connecting both apices mesially. Both pulp cavities are moderately taurodontic (Gorjanovic-Kramberger, 1907, 1908; Garralda et al., 2023), extending to the points of bifurcation (SOM Fig. S4).

The P^3 has an elongated crown outline, wider buccally but symmetric mesiodistally. The worn occlusal relief is discernible through the sulci. The sagittal sulcus seems to interrupt the transverse crest (grade 1; SOM Table S5b). A short anterior fovea is visible. Distally, a lateral sulcus is present on the Pa, attesting the presence of a lateral accessory ridge.

At the EDJ, the essential crest is continuous (grade 2; SOM Table S5b). The mesial marginal ridge is acute and high and remains uninterrupted until it flattens at the Pro dentine horn, whereas the distal marginal ridge flattens in a notch lingually. Furthermore, the Pa distal accessory ridge seems bifurcated.

Right maxilla fragment: C^1–M^3 #46 The maxilla fragment preserves the C^1 to the M^3, whereas the bone is shortened anteroposteriorly until only the periradicular alveolar bone remains on the M^3 (Table 1; Fig. 12; David et al., 2009; Tillier et al., 2013a). All the teeth are complete, except for a distolingual break of the M^1. Every tooth presents traces of supragingival calculus buccally and lingually. Each root presents apical hypercementosis, increasingly higher as we progress posteriorly, with the M^3 hypercementosis on almost half of the root height. Occlusal wear is also not uniform across the teeth, with the M^1 more worn (stage 5; Table 1) and the M^3 less worn (stage 3; Table 1) than the other teeth (stage 4; Table 1). Furthermore, the M^3 occlusal relief is slightly displaced buccally compared to the other molars. A beveled wear facet is marked distally on the P^4 and first 2 Ms but especially on the M^1. On the C^1 and P^3, the wear facet is slightly convex oblique wear. Moreover, the C^1 and P^3 show an important occlusal pitting of the lingual enamel edge, with lingual chipping for the canine. Lastly, a small toothpick grove is suspected buccodistally on the cervical part of the M^1 root (white arrow, Fig. 12), without stigmata transferred on the M^2. The individual seems to be a middle-aged adult.

The lingual profile of the C^1 exhibits a pronounced convexity (cyrtodont), accentuated by hypercementosis that enhances the overall root appearance, which is notably round and homogeneous. The crown is labially convex except for a distal asymmetry that extends the crown into a flatter surface. The other crown structures are worn; thus, the seemingly large marginal ridge morphologies are not discernible. The cingulum is pronounced (Bushman canine, grade 2; tuberculum dentale, grade 5; SOM Table S3) and is notably isolated by a distal coronoradicular groove and a sulcus perpendicular to the deep central one.

At the EDJ, the distal half of the labial face of the crown is marked by a discernible convexity. The apex of the cusp is mesially placed, with the essential crest near the mesial marginal ridge, leaving a deep groove distally. The marginal ridges are neatly protruding and mark a notch before the deep sulcus isolating the cingulum, especially distally. The cingulum is isolated, with a mild marginal ridge and a high dentine horn.

The P^3 root buccal profile exhibits a corrugated appearance, but the overall buccal profile of the tooth is slightly convex with the globular crown. The roots are divided midway, with a pronounced groove distally that almost extends to the cervix, and a cementum junction joins them mesially leaving only the apices free. There is no extension of the pulp cavity (SOM Fig. S4). The crown occlusal reliefs seem symmetric, with a central transverse crest, delineated by two foveae mesially and distally. A concavity is noticeable mesially on the lingual wall.

At the EDJ, the crown symmetry appears less pronounced, and the transverse crest is weakly expressed (grade 2; SOM Table S4). The essential crests of the cusps are not visible due to occlusal wear and tooth fractures. Lingually, the distal marginal ridge is rounded, and the Pro is mesially placed. The mesial marginal ridge forms a small protrusion at the central sulcus and is reduced at the Pro compared to the distal one. The mesial and distal grooves lack complexity. Finally, the lingual wall concavity is clearly expressed at the EDJ.

The P^4 buccal profile is convex (cyrtodont), and its roots are entirely fused. The pulp cavity reveals two free apices following an enlarged cavity buccolingually (SOM Fig. S4), which could be considered as an extreme form of taurodontism (SOM Fig. S4). The occlusal structures are asymmetrically distributed, with the notably mesial position of the Pro. The Pa does not present any distal lateral accessory ridges (grade 0; SOM Table S4), but distal structures seem to occupy a large portion of the crown distolingually. The sagittal sulcus neatly interrupts the transverse crest (grade 0; SOM Table S4).

At the EDJ, the marginal ridge seems continuous, and no accessory or central ridging is visible (respectively grade 0; SOM Table S4). However, two horn-like thickenings of the ridge are expressed distally: one at the center of the Pa distal marginal ridge and another nearly aligned with the sagittal groove.

The mesial side of the M^1 is oriented distally, and the apices of the three individualized roots exhibit an overall upward direction. The tooth presents an asymmetric crown contour, with the Hyp larger than the other cusps (Hyp > Pro > Pa > Met). The crista obliqua (grade 1; SOM Table S5b) seems expressed, along with a mesial complexity. Linguomesially, the Pro wall shows a marked convexity, a groove likely accompanied by a lateral ridge.

At the EDJ, the marginal ridge is worn, but it seems to protrude at the Hyp, featuring a groove that marks the intercuspation. Additionally, an accessory horn tip might be expressed on the marginal ridge distally from the Met.

The upper halves of the M^2 roots converge distally, with three close roots maintaining independent apices. The nearly square crown exhibits four main discernible cusps (Pa > Pro > Met > Hyp) but lacks accessory structures at the occlusal surface. Slight enamel extensions are present buccally and lingually.

At the EDJ, a continuous crista obliqua (grade 1; SOM Table S5b) connects the Met dentine horn to the Pro via its lateral marginal ridge. An accessory ridging is well expressed on the mesial marginal ridge, whereas a barely discernible ridge is observed on the distal marginal ridge. The Hyp essential crest connects with the Pro distal ridge, forming an angular ridge with the marginal ridge that flattens toward the dentine horn. The Hyp presents two lateral ridges mesially, one connecting to the Pro and one flattening into the buccal wall and borders the intercuspal groove that aligns with the distal sulcus to the crista obliqua.

The M^3 roots are fused, and connecting apices are joined with hypercementosis nodules. Furthermore, the roots are in alignment with the crown walls. The tooth crown structures are more developed mesially, with a large protruding Pa. However, the Hyp is well expressed (Pa > Pro > Hyp > Met). A C6 and C7 may be expressed as well as mesial tuberosities, and a small Carabelli's is present (grade 2; SOM Table S5b). No crista obliqua is present (grade 1; SOM Table S5b), and structures are separated by deep sulci.

At the EDJ, there is no anterior fovea, but an important groove is expressed mesially from the Pa and buccally from the pronounced ridging of the mesial marginal ridge. The Pa essential crest is

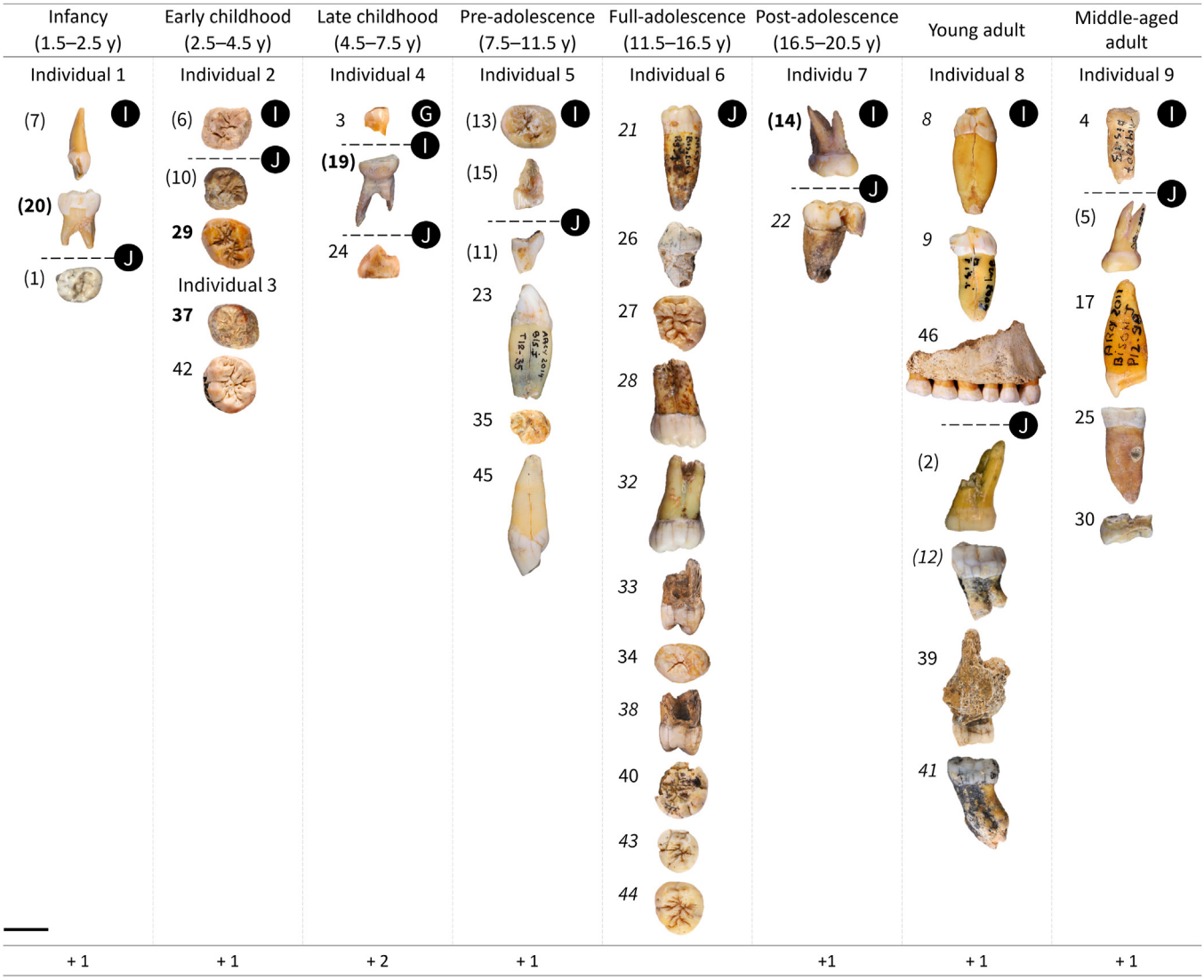

Figure 13. The Grotte du Bison dental collection, organized by age class, showing the minimal number of individuals. For each age class, the stratigraphic unit is detailed (layer G, I, and J), with the possibility of additional individuals represented in each age group. The tooth position repetitions are indicated in bold (with the left dP_4 and right M^1). The paired individuals are in italics. The previously published individuals are in parentheses. Scale = 5 mm (except for #46). y = years.

bifurcated, and a marked accessory ridge is present, with a high dentine horn at the marginal ridge. The Met is isolated by a deep groove that extends from the sagittal sulcus. Accessory dentine horns are well expressed distally from the Met at the C5 and at the center of the Pro distal accessory ridge. The ridge of the C5 and the distal accessory ridge of the Pro join together and isolate the Hyp. The Hyp apex is elevated from the surrounding marginal ridges, and the buccal intercuspal area presents a deep concavity created by an outer ridging of the two cusps.

4. Discussion

4.1. Tooth collection and dental associations

The most common hominin remains are two right deciduous P_4s for the immature individuals and up to four right M^1s for the mature ones. There are no multiple postcranial or cranial bone fragments from the same skeletal element.

Considering the most common teeth and developmental age, we can estimate a minimum of nine individuals (one infant, three children, three adolescents, and two adults; Fig. 13). Uncertainties in molar positions do not impact the minimum number of individuals. If #13 and #27 are third molars, they would be in their postadolescence at death and #28 and #32 would be young adult individuals (Fig. 13). If #22 is a first molar, it would still be associated to an adolescent (Fig. 13). Additionally, if we consider the distribution of the remains within the three archaeological layers, 17 individuals may be represented (Table 1; Fig. 13).

Moreover, some teeth can be associated with the same individual. In the layer I, the right C_1 #8 and right P_3 #9 are found in two adjacent fieldwork square meters (R10 and R11) and show the same preservation state (similar coloration and frontal fracture; Figs. 9 and 10). Most importantly, there is an exact matching of their corresponding interproximal contact facets and occlusal wear (Fig. 14). The canine shows a convex distal facet that dips lingually and joins a mesial oblique wear facet on the buccal side of the premolar.

In layer J, there is a total of five pairings. The left M_2 #41 and M_3 #12 are found more than 5 m away from each other (Q11 and P7, respectively). However, they have similar morphologies and taphonomic effects (flaky cementum and manganese; Fig. 11), and their

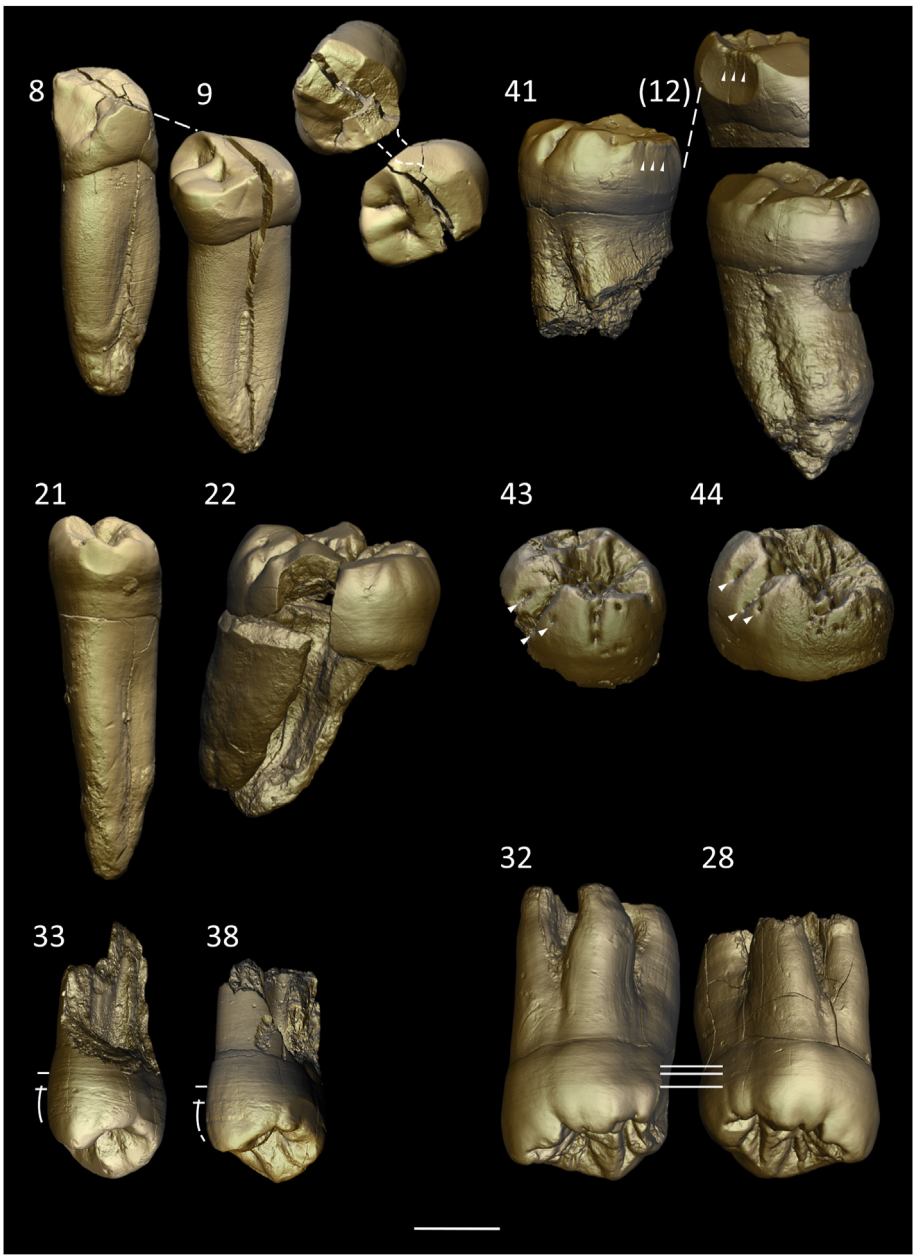

Figure 14. The paired specimens: RC_1 #8 and RP_3 #9; LM_2 #41 and LM_3 #12; RP_4 #21 and $LM_{2/1}$ #22; LM_2 #43 and LM_3 #44; RP^3 #33 and RP^4 #38; $LM^{2/3}$ #32 and $RM^{2/3}$ #28. The canine and premolars are presented in the distolingual view, and the molars are in the buccodistal view. The dotted lines show the interproximal wear facets connections and the corresponding occlusal wear facet for #8 and #9. The arrows indicate the subvertical grooves on #41 and #12 interproximal wear facets and some matching hypoplasic pits on #43 and #44. Finally, the plain lines highlight corresponding perikymata on #33–#38 and #32–#28, with curved lines indicating hypoplasic events on #33–#38. The previously published tooth is in parenthesis. Scale = 5 mm.

common interproximal contact facets present perfectly matching subvertical grooves (the largest three are evident in Fig. 14).

The left M_2 #43 and left M_3 #44 were extracted from the same concretion block (x = 15.845, y = 10.575, z = −1.78; following the [0,x] and [0,y] axes of the fieldwork grid) measuring approximately 5 on 3 cm upon extraction (also considered as an argument for the rank attribution of #43 as the tooth was found in the mesial position from #44). Additionally, these teeth present highly similar morphologies (especially the conformation and wrinkling of the OES cusps; Fig. 11) and numerous pitted hypoplasias with an almost identical repartition (Fig. 14). The P^3 #33 and P^4 #38, respectively, from squares S8 (x = 19.329, y = 8.39, z = −1.461) and P8 (x = 16.555, y = 8.492, z = −1.792), share similar taphonomic degradations and root breakage (Fig. 7). They have highly similar morphologies with well-developed structures, a small interproximal contact facet, and similar developmental features. Important hypoplasic events are expressed in the upper half of the crowns, and the perikymata are clearly visible (Fig. 14). The perikymata are frequently expressed in paired patterns, and matching can be done with the highest ones (SOM Fig. S6) while considering the difference in their developmental period.

Finally, antimeres are identified in the sample, specifically the left $M^{2/3}$ #32 and right $M^{2/3}$ #28, respectively, from P11 (x = 16.01, y = 11.054, z = −1.797) and O9 (x = 15.816, y = 9.146, z = −1.534). The right molar is more taphonomically impacted; thus, we assume that the broken roots of #28 were identical to #34. However, they

maintain an almost identical morphology down to their perikymata expression (Figs. 8 and 13). Variation in this expression is evident at a microscopic scale, especially with hypoplasic occurrences (detailed in SOM Figs. S6c and d).

Other teeth could potentially be associated with the same individuals, with less reliable evidence than previous demonstrations. For example, the right P_4 # 21 and left $M_{2/1}$ #22 have similar taphonomic weathering and manganese incursions (Figs. 10 and 11) and were excavated together from the R9 square (x = 18.198, y = 9.207, z = −1.693 and x = 18.187, y = 9.34, z = −1.711, respectively). The right $M^{1/2}$ #14 and right $M^{2/3}$ #13 could belong to the same individual as they have similar EDJ morphology and similar chemical degradation (Fig. 8). It is important to note that every specimen presenting biochemical degradation such as partial digestion is from layer I (#19, #13, #14, #4, #5). No pairings are identified between specimens recovered from the different layers.

4.2. The Grotte du Bison dental morphologies and Neandertal variability

This analysis includes both permanent and deciduous teeth, highlighting distinctive Neandertal characteristics (trait expression in SOM Tables S2–S5) and examining their crown diameters (SOM Table S6) within the variability of Middle and Upper Pleistocene Neandertals and Upper Pleistocene modern humans (SOM Fig. S7).

The upper incisors (Fig. 6) show labial convexity (100% grade 4; compared to 47.6% grade 4 for 21 Neandertal I^1s and 64.6% grade 5 for 20 Neandertal I^2s; Martinón-Torres et al., 2012) and pronounced shoveling (two grade 4 and one grade 5; compared to 33.3% grade 5 for 21 Neandertal I^1s and 41.9% grade 5 for 31 Neandertal I^2s; Martinón-Torres et al., 2012). The shoveling is more similar to la Sima de los Huesos individuals than to the comparative Neandertal and Middle Pleistocene humans from the Martinón-Torres et al. (2012) comparative sample. The deciduous tooth #7 expresses the same morphology (Fig. 4), even though the tuberculum dentale is absent (grade 1 for the deciduous tooth and grade 4 for the permanent teeth; compared to 52.4% grade 4 for 21 Neandertal I^1s and 40% grade 5 for 30 Neandertal I^2s; Martinón-Torres et al., 2012). These traits are expressed more moderately at the EDJ (SOM Table S2). Furthermore, a faint double shoveling for tooth #11 is expressed at the EDJ, but it is absent from the OES.

The Grotte du Bison specimen #11 and the left I^1 from the Grotte de l'Hyène (Leroi-Gourhan, 1958) are very close in size (SOM Fig. S7). They are within the Neandertal range of variation and are shorter mesiodistally than the Atapuerca individuals. As for #45, the tooth is on the upper end of the Neandertal range, close to the largest central incisor from Krapina (KDP 2 and 6).

The canines have a highly convex buccal profile (cyrtodont), with elongated roots for the upper canines, exacerbated by apical hypercementosis (#17 and #46; Figs. 6 and 12; SOM Fig. S4; Le Cabec et al., 2013). They also have developed crown features and accessory tubercle. The #46 C^1 is moderately shoveled with a cusp-like tuberculum dentale (respectively: 40.9% grade 3 and 4 for 21 Neandertal C^1s; 33.3% grade 5 for 21 Neandertal C^1s; Martinón-Torres et al., 2012). The dC^1 #15 also has a well-expressed cingulum with a tubercular expression isolated from the developed marginal ridges. The C_1 #23 has a moderate shovel shape and pronounced ridging (40% grade 3 for 25 Neandertal C_1s; 52% grade 0 for 25 Neandertal C_1s; Martinón-Torres et al., 2012), with a developed distal accessory ridge (50% grade 2 for 9 Neandertal C_1s; Martinón-Torres et al., 2012), especially visible on the EDJ for #8 and #23 (SOM Table S3). However, the dC_1 #3 is gracile and lacks significant structures. Moreover, the anterior permanent teeth display distal subhorizontal accessory ridges (#45 and #8; Figs. 6 and 9) or a protruding distal marginal ridge (#11 and #23; Figs. 6 and 9). Lastly, on the buccal view of the upper and lower permanent canines (#17 and #23; Figs. 6 and 9), a pronounced and deep horizontal concavity is observed on both the OES and the EDJ. It remains to be determined whether this feature is a nonspecific stress mark or a biomechanical consequence secondary to dental or other biological overcrowding during tooth development.

The dimensions of the upper and lower canines from the Grotte du Bison and Grotte du Renne are within the Neandertal variability, and smaller than the early and pre-Neandertals (SOM Fig. S7). The #17 is distally worn but is buccolingually much smaller than the Neandertal and fossil modern human variability. The dC_1 #3 is small compared to the Grotte du Renne dC_1 #78 but bigger than the La Ferrassie 8 and Chateauneuf 2 Neandertals.

The premolars are highly diagnostic. The P^3s have bifurcated lingual crests (Fig. 7) and interrupted transverse crests at the OES (grade 0: 93.3% for 16 Neandertal P^3s; Martinón-Torres et al., 2012), which are continuous at the EDJ. The P^4s have mesially placed essential crests and buccodistal accessory ridges. Distal bifurcation of essential crests is observed on the Pa of #33 and #38, and on the Pro of #24 (Figs. 7 and 10), with a corresponding development at the EDJ for the upper premolars. The expression of the distal accessory ridge at the OES is highly variable, especially for the lower premolars. Lower premolars have two lingual cusps, characteristic of Neandertal, showing multiple lingual cusps (grade 3 in 25.9% and grade 4 in 29.6% for $n = 27$ Neandertal P_3s; grade 4 in 70.4% for $n = 27$ Neandertal P_4s; Martinón-Torres et al., 2012). The P_3s have continuous or lingually expressed transverse crests. Mesial grooves are present on the buccal side of the P_3s (grade 1 in 57% 14 Neandertals P_3s; Davies et al., 2019). The P_4s present overall developed ridges and crown asymmetry as seen in Neandertals but weak transverse crests similar to the Middle Pleistocene expression (mesial Met placement: 96.9% in 32 Neandertal P_4s; asymmetric crown contour: 93% for 31 Neandertal P_4s; Bailey, 2006; transverse crest: grade 2 in 75% for 26 Neandertal P_4s, and grade 1 in 60% for 5 pre-Neandertals; Martinón-Torres et al., 2012). The marginal ridge is continuous in 50% of the lower premolars, directed outward from the occlusal bassin at the EDJ, as the ridge is strongly developed at the OES. The upper premolar roots are overall taurodont (SOM Fig. S5; Keen, 1966; Kupczik and Hublin, 2010). The cementum bridge between the roots and the spacing of root apices is variable, reflecting the taurodont expression. The second maxillary premolar exhibits a greater degree of taurodontism, characterized by closer apices and thicker cementum development. In the maxilla #46, the P^4 external root morphology appears monoradicular. The fused roots, however, are revealed by an enlarged pulp cavity mesiodistally, with two canals present apically. This mesotaurodontism to hypertaurodontism is also observed in the Neandertal specimen El Castillo-1466 left P^4 (Garralda et al., 2023).

The Grotte du Bison P^3s are big, especially compared to the Middle and Upper Pleistocene variability (SOM Fig. S7). The hemimaxilla #46 notably shows a big P^3 compared to the Neandertal variability, but especially compared to the proportion of the other teeth of the maxilla, falling on the lower side of the Neandertal variability. The P^4s are not as large except for #30, which displays a large buccolingual diameter compared to the mesiodistal one. The lower premolars display large dimensions as well (such as the Grotte de l'Hyène individuals), especially #9 and #21 based on the comparative sample variability (with larger buccolingual and mesiodistal diameters, respectively).

The deciduous premolars and permanent molars show a homogeneous expression of accessory structures and structure complexity (SOM Fig. S8). A small C5 is present on the upper molars, with a highly variable expression in the third molars

(compared to grade 2 at 45.5% and 40%, respectively, for 22 Neandertal M^1s and 20 M^2; and grade 0 at 35.5% for17 Neandertal M^3s; in Martinón-Torres et al., 2012). Furthermore, cusp-like accessory ridges are expressed distally from the Pa and Pro (Fig. 8). Mesial marginal accessory tubercles are expressed, even faintly for the left dP^4 #1 and the $M^{2/3}$s #28 and #32 (grade 1 at 63.2% for 19 Neandertal M^1s, 81.3% for 16 Neandertal M^2s, and 85.7% for 14 Neandertal M^3s; Martinón-Torres et al., 2012). Either the crista obliqua is continuous, connecting the Pro and Met horn tips (33%), or the Met essential crest fades between the Pro essential crest and distal accessory ridge (44%; SOM Fig. S8). For the right M^1 #14, the Met essential crest joins the Pro distal accessory ridge. Carabelli expressions are present on both deciduous premolars but only the M^3 #34 for permanent teeth (a more tubercular expression mesially from the Pro distal accessory ridge of #5). However, at the EDJ, upper molars are complex lingually, with ridging mesially from the Hyp to the Pro. On the M^1s the Hyp is linguodistally isolated from the square crown outline, creating a more developed ridge mesially from the cusp and a deeper sulcus (Fig. 8). The M^2s #2 and #13 also present some lingual ridging, especially at the Pro distal accessory ridge, but the cusps' expression at the lingual wall is far less pronounced (as opposed to the 'B' shape of the M^1 occlusal crown contour; Fig. 8; SOM Fig. S8). Finally, every Pa and Met presents an accessory dentine horn distally, except for the M^3 (SOM Fig. S8).

The lower molar C6 and C7 are more markedly expressed on the M_2s and M_3s, with an overall stronger expression of C7 (in Martinón-Torres et al., 2012, the C6 and C7 are absent in Neandertal third molar 30% and 50% of the time, respectively; Fig. 11). This is also observed on the deciduous premolar #20 (Fig. 5). The anterior fovea of the lower molars and lower deciduous premolars is formed with developed mesial marginal ridges, and mid-trigonid crests that features centrally placed tubercular expressions on the Pro essential ridge (expressed at the EDJ by an accessory dentine horn; Fig. 11; SOM Fig. S8). The protostylid is expressed on the M_2s #22, #40, and #41, and only a deep intercuspal groove is present on the other molars (61.5%–96.8% grade 0 for Neandertal M_3 to M_1; Martinón-Torres et al., 2012). At the EDJ, the tubercular expression on the Pro and Hyp intercuspation reflects the OES expression (#22, #41, and #44; Fig. 11; SOM Fig. S8). The M_1 presents marked intercuspal grooves on the buccal wall, extending in a continuous convexity that surrounds the height of the cusps. The buccal side of the other lower molars is highly complex, with a tubercular expression mesially from the C5 (57%) or distally from the Hyp (28%). However, there is more accessory dentine horn expression linguodistally. Another trait visible at the lower molar EDJ is the centrally displaced Met dentine horn, especially marked in the first molars (SOM Fig. S8).

The deciduous premolars from the Grotte du Bison are relatively small and fall in the lower end of the overlapping Middle and Upper Pleistocene variability (SOM Fig. S7). The Grotte du Bison upper molars display highly variable dimensions but stay in the center of the fossil variability (SOM Fig. S7). The $M^{2/3}$s #28 and #32 are slightly bigger and close to Spy 2 and Shanidar 2 M^2s. The maxilla #46 M^2 and M^3 #29 are relatively small. However, the latter is particularly small due to reduced lingual cusps and the centrally placed Met. The lower M_1s are bigger than Arcy-sur-Cure teeth and the Neandertal distribution, with #22 being bigger than Krapina specimens (close to Krapina 3). The other molars fit well with Neandertal variability, with slightly larger mesiodistal diameters for the M_3 #44 and a left M_3 from the Grotte de l'Hyène. The M_3 #12 rounded morphology makes it fall toward the highest Neandertal buccolingual diameters compared to the mesiodistal ones, such as Spy 1, Ochoz 1, and Zafaraya 2, but not as pronounced as the Bañolas specimen.

Lastly, a notable occurrence in Grotte du Bison dental remains are developmental patterns, such as potential ameloblast resorption-induced pitting and grooves on the cusp and marginal ridges apices, during enamel maturation (cf. #1, #10, #20, #21, #42, #43, and maybe #6 and #29; Figs. 5, 8, 10, and 11). This pattern is present on many teeth from Arcy-sur-Cure caves and was first observed on previously published deciduous premolars from the Grotte du Renne, where the deformations are especially marked (Henrion et al., 2023).

5. Conclusions

This study builds on previous research regarding the human remains of Arcy-sur-Cure, such as the work of Bailey and Hublin (2006) on the Grotte du Renne Châtelperronian associated dental remains, and the work of Tillier et al. (2013a, 2013b) on slightly older human fossils discovered in its geological twin cavity, the Grotte du Bison. This site is significant due to its rich collection of human fossils primarily concentrated in two Mousterian layers (I and J). Here, we present results of the first comprehensive analysis of this site, broadening our understanding of this unique Neandertal settlement in northeastern France during the Upper Pleistocene.

A minimum of nine individuals are represented in the Grotte du Bison. Almost every age at death is represented except perinatal, with a prevalence of young individuals, including children and adolescents, and fewer adults. We identified five to six pairings among the young adult and adolescent individuals. They are primarily concentrated in layer J, except for one pairing in layer I. These remains exhibit distinctive taphonomic alterations and developmental features but variable horizontal and vertical dispersions within the cave. However, no interlayer matching of specimens is evident. On the other hand, it is noteworthy that the dental remains with tissue modifications caused by digestion are concentrated in the layer I.

Several teeth and their dental ranks were identified through their internal morphologies. Notably, some molars and premolars exhibit high levels of acidic and biochemical modifications, taphonomic alterations, and heavy occlusal wear. The P_4s display multiple lingual pulp horns and distinctive EDJ morphologies (with an anterior fovea and a marked distal basin). The molars showed complex occlusal reliefs at the EDJ and characteristic marginal ridge elevations, which at the OES were often worn or not discernible due to the immature enamel in deciduous teeth.

Morphological homogeneity was evident in the molars, the dental class most represented in our sample. We observed a high recurrence of accessory structures such as distal accessory ridges to the Pa and Pro, often associated with accessory dentine horns at the marginal ridge. Upper molars frequently presented a fovea mesially from the Pa, whereas lower molars exhibited accessory tubercles on the buccal wall, primarily on the Hyp and/or C5. Furthermore, the I^1 and P^3 were especially diagnostic, with large morphological structures. The premolar roots showed high variability, especially the maxillary premolars, with different taurodontic expression and root fusion. Further studies are needed to record this variability in Middle and Upper Pleistocene individuals.

The Arcy-sur-Cure Neandertals present homogenous morphologies, likely reflecting the narrow chronological interval of the cave occupations. Throughout the Arcy-sur-Cure collections, especially in deciduous premolars and germs of permanent teeth, developmental patterns are identified as potential ameloblast resorption pits and grooves on the cusp apices and marginal ridge, requiring further investigation. Finally, Arcy-sur-Cure Neandertals also exhibit distal wear basins, with severe angular expressions in several individuals from the Grotte du Bison and the Grotte de l'Hyène. A study of the

worn dental remains from the Arcy-sur-Cure caves is necessary for understanding the different wear mechanics and, ultimately, individual paramasticatory and nonmasticatory behaviors.

Declaration of competing interest

The authors declare no conflict of interests.

Acknowledgments

We would like to thank the Régional Service of Archeology of Bourgogne-Franche-Comté (Y. Pautrat), the Musée National de Préhistoire—Les Eyzies (dir. J-J. Cleyet-Merle and now N. Fourment), for granting access to the original remains and H. Temming (Max Planck Institute [MPI]) for granting us the access to the computed tomography scans of the two Grotte du Bison fossils. We are thankful to M. Julien and M. Girard for discussions about Leroi-Gourhan's fieldwork at Arcy-sur-Cure. We are deeply grateful to M. Bessou for the photography of some remains and to A. Le Cabec for her availability and for access to VG Studio. We are also grateful to the Editor, Associate Editor, and reviewers for their help in improving our paper. This project was supported by UMR PACEA and ArScAn, funded by a CNRS MITI PhD grant (J. Henrion) and the Région Nouvelle Aquitaine scientific project ADNER (codir. P. Bayle and B. Maureille, convention no. AAPR2021-2020-11779310). This research benefited also from the scientific framework of the University of Bordeaux's IdEx 'Investments for the Future' program/GPR 'Human Past' and PACEA scientific teams 'EuraPal' and 'Evo-DiBio' (M. Augoyard, A. Arzelier, S. Blunt, S. Garcia Liebana, D. López Onaindia, N. Martin, and C. Zanolli).

Author contributions

Juliette Henrion: Writing – review & editing, Writing – original draft, Visualization, Methodology, Investigation, Formal analysis, Conceptualization. **Bruno Maureille:** Writing – review & editing, Supervision, Project administration. **Cédric Beauval:** Writing – review & editing, Resources, Data curation. **Nicolas Vanderesse:** Writing – review & editing, Resources, Data curation. **Jean-Jacques Hublin:** Writing – review & editing, Supervision, Project administration. **Maurice Hardy:** Writing – review & editing, Funding acquisition, Data curation.

Supplementary Online Material

Supplementary Online Material related to this article can be found at https://doi.org/10.1016/j.jhevol.2024.103631.

References

AlQahtani, S.J., Hector, M.P., Liversidge, H.M., 2010. Brief communication: The London atlas of human tooth development and eruption. Am. J. Phys. Anthropol. 142, 481–490. https://doi.org/10.1002/ajpa.21258.

AlQahtani, S.J., Hector, M.P., Liversidge, H.M., 2014. Accuracy of dental age estimation charts: Schour and Massler, Ubelaker and the London Atlas: Accuracy of three dental charts. Am. J. Phys. Anthropol. 154, 70–78. https://doi.org/10.1002/ajpa.22473.

Baffier, D., Girard, M., 1997. Le karst d'Arcy-sur-Cure (Yonne) et ses occupations humaines paléolithiques. Quaternaire 8, 245–255. https://doi.org/10.3406/QUATE.1997.1577.

Bailey, S.E., 2002a. Neandertal Dental Morphology: Implications for Modern Human Origins. Ph.D. Dissertation, Arizona State University.

Bailey, S.E., 2002b. A closer look at Neanderthal postcanine dental morphology: The mandibular dentition. Anat. Rec. 269, 148–156. https://doi.org/10.1002/ar.10116.

Bailey, S., 2006. Beyond shovel-shaped incisors: Neandertal dental morphology in a comparative context. Period. Biol. 108, 253–267.

Bailey, S.E., Hublin, J.-J., 2006. Dental remains from the Grotte du Renne at Arcy-sur-Cure (Yonne). J. Hum. Evol. 50, 485–508. https://doi.org/10.1016/j.jhevol.2005.11.008.

Bailey, S.E., Skinner, M.M., Hublin, J.-J., 2011. What lies beneath? An evaluation of lower molar trigonid crest patterns based on both dentine and enamel expression. Am. J. Phys. Anthropol. 145, 505–518. https://doi.org/10.1002/ajpa.21468.

Bastir, M., Rosas, A., García Tabernero, A., Peña-Melián, A., Estalrrich, A., de la Rasilla, M., Fortea, J., 2010. Comparative morphology and morphometric assessment of the Neandertal occipital remains from the El Sidrón site (Asturias, Spain: years 2000–2008). J. Hum. Evol. 58, 68–78. https://doi.org/10.1016/j.jhevol.2009.08.006.

Belcastro, M.G., Mariotti, V., Riga, A., Bonfiglioli, B., Frayer, D.W., 2018. Tooth fractures in the Krapina Neandertals. J. Hum. Evol. 123, 96–108. https://doi.org/10.1016/j.jhevol.2018.06.009.

Brothwell, D., 1989. The relationship of tooth wear to aging. In: Iscan, M.Y. (Ed.), Age Markers in Human Skeletons. Charles C. Thomas Publisher, Ltd., Springfield, pp. 303–316. https://doi.org/10.1016/j.jasrep.2022.103707.

Byers, S.N., 2002. Introduction to Forensic Anthropology: A Textbook. Allyn and Bacon, Boston.

Chapple, A.S., Skinner, M.M., 2023. A tooth crown morphology framework for interpreting the diversity of primate dentitions. Evol. Anthropol. 32, 240–255. https://doi.org/10.1002/evan.21994.

David, F., Connet, N., Girard, M., Miskovsky, J.-C., Mourer-Chauviré, C., Roblin-Jouve, A., 2006. Les niveaux du Paléolithique supérieur à la grotte du Bison (Arcy-sur-Cure, Yonne): Couches a à d. Rev. Archéol. Est 54, 5–50.

David, F., Connet, N., Girard, M., Miskovsky, J.-C., Mourer-Chauviré, C., Roblin-Jouve, A., 2006. Les niveaux du Paléolithique supérieur à la grotte du Bison (Arcy-sur-Cure, Yonne) : couches a à d. Rev. Archéol. Est. 54, 5–50.

David, F., D'Iatchenko, V.I., Enloe, J.E., Girard, M., Hardy, M., Lhomme, V., Roblin-Jouve, A., Tillier, A.-M., Tolmie, C., 2009. New Neandertal remains from the Grotte du Bison at Arcy-sur-Cure, France. J. Hum. Evol. 57, 805–809. https://doi.org/10.1016/j.jhevol.2009.03.006.

Davies, T.W., Delezene, L.K., Gunz, P., Hublin, J.-J., Skinner, M.M., 2019. Endostructural morphology in hominoid mandibular third premolars: Discrete traits at the enamel-dentine junction. J. Hum. Evol. 136, 102670. https://doi.org/10.1016/j.jhevol.2019.102670.

Dean, C., Leakey, M.G., Reid, D., Schrenk, F., Schwartz, G.T., Stringer, C., Walker, A., 2001. Growth processes in teeth distinguish modern humans from *Homo erectus* and earlier hominins. Nature 414, 628–631. https://doi.org/10.1038/414628a.

Dean, D., Hublin, J.-J., Holloway, R., Reihard, Z., 1998. On the phylogenetic position of the pre-Neandertal specimen from Reilingen, Germany. J. Hum. Evol. 34, 485–508. https://doi.org/10.1006/jhev.1998.0214.

Devièse, T., Abrams, G., Hajdinjak, M., de Groote, I., Di Modica, K., Toussaint, M., Fischer, V., Comeskey, D., Spindler, L., Meyer, M., Semal, P., Higham, T., 2021. Reevaluating the timing of neanderthal disappearance in northwest europe. Proc. Natl. Acad. Sci. USA 118, e2022466118. https://doi.org/10.1073/pnas.2022466118.

Dodat, P.-J., Albalat, E., Balter, V., Couture-Veschambre, C., Hardy, M., Henrion, J., Holliday, T., Maureille, B., 2024. Diverse bone-calcium isotope compositions in Neandertals suggest different dietary strategies. J. Hum. Evol. 193, 103566. https://doi.org/10.1016/j.jhevol.2024.103566.

Fuchs, J., García-Tabernero, A., Rosas, A., Camus, H., Metz, L., Slimak, L., Zanolli, C., 2024. The dentition of a new adult Neanderthal individual from Grotte Mandrin, France. J. Hum. Evol. 196, 103599. https://doi.org/10.1016/j.jhevol.2024.103599.

Garralda, M.D., Le Cabec, A., Maíllo Fernández, J.M., Maureille, B., Gunz, P., Neira, A., Hublin, J.-J., Bernaldo de Quirós, F., 2023. Mousterian human fossils from El Castillo cave (Puente Viesgo, Cantabria, Spain). J. Anthropol. Sci. 101, 123–142. https://doi.org/10.4436/JASS.10021.

Girard, M., Miskovski, J.-C., Evin, J., 1990. La fin du Würm moyen et le début du Würm supérieur à Arcy-sur-Cure (Yonne): Précisions paléoclimatiques et chronostratigraphiques d'après le remplissage de la grotte. In: Farizy, C.Dir (Ed.), Paléolithique moyen et Paléolithique supérieur ancien en Europe. Actes du colloque international de Nemours, Mémoires du Musée de Préhistoire d'Ile-de-France, Nemours, pp. 295–303.

Gorjanovic-Kramberger, K.D., 1907. Die Kronen und Wurzeln der Mahlzähne des *Homo primigenius* und ihre Genetische Bedeutung. Anat. Anzeiger 31, 97–134.

Gorjanovic-Kramberger, K.D., 1908. Uber prismatische Molarwurzeln rezenter und diluvialer Menschen. Anat. Anzeiger 32, 401–413.

Gravina, B., d'Errico, F., Bachellerie, F., 2022. Disentangling Neanderthal-modern human interactions in Western Europe: A heuristic odyssey. In: Clack, T., Brittain, M. (Eds.), Archaeologies of Cultural Contact: At the Interface. https://doi.org/10.1093/oso/9780199693948.003.0006. Oxford.

Gray, H., Standring, S., Anhand, N. (Eds.), 2021. Gray's Anatomy: The Anatomical Basis of Clinical Practice, 42nd ed. Elsevier, Amsterdam.

Hajdinjak, M., Fu, Q., Hübner, A., Petr, M., Mafessoni, F., Grote, S., Skoglund, P., Narasimham, V., Rougier, H., Crevecoeur, I., Semal, P., Soressi, M., Talamo, S., Hublin, J.-J., Gušić, I., Kućan, Ž., Rudan, P., Golovanova, L.V., Doronichev, V.B., Posth, C., Krause, J., Korlević, P., Nagel, S., Nickel, B., Slatkin, M., Patterson, N., Reich, D., Prüfer, K., Meyer, M., Pääbo, S., Kelso, J., 2018. Reconstructing the genetic history of late Neanderthals. Nature 555, 652–656. https://doi.org/10.1038/nature26151.

Henrion, J., Hublin, J.-J., Maureille, B., 2023. New Neanderthal remains from the Châtelperronian-attributed layer X of the Grotte du Renne (Arcy-sur-Cure, France). J. Hum. Evol. 181, 103402. https://doi.org/10.1016/j.jhevol.2023.103402.

Higham, T., Douka, K., Wood, R., Bronk Ramsey, C., Brock, F., Basell, L., Camps, M., Arrizabalaga, A., Baena, J., Barroso-Ruíz, C., Bergman, C., Boitard, C., Boscato, P., Caparrós, M., Conard, N.J., Draily, C., Froment, A., Galván, B., Gambassini, P., Garcia-Moreno, A., Grimaldi, S., Haesaerts, P., Holt, B., Iriarte-Chiapusso, M.-J., Jelinek, A., Jordá Pardo, J.F., Maíllo-Fernández, J.-M., Marom, A., Maroto, J., Menéndez, M., Metz, L., Morin, E., Moroni, A., Negrino, F., Panagopoulou, E., Peresani, M., Pirson, S., de la Rasilla, M., Riel-Salvatore, J., Ronchitelli, A., Santamaria, D., Semal, P., Slimak, L., Soler, J., Soler, N., Villaluenga, A., Pinhasi, R., Jacobi, R., 2014. The timing and spatiotemporal patterning of Neanderthal disappearance. Nature 512, 306–309. https://doi.org/10.1038/nature13621.

Hillson, S., 1996. Dental Anthropology. Cambridge University Press, Cambridge.

Hublin, J.-J., 2009. The origin of Neandertals. Proc. Natl. Acad. Sci. USA 106, 16022–16027. https://doi.org/10.1073/pnas.0904119106.

Hublin, J.-J., 2012. The earliest modern human colonization of Europe. Proc. Natl. Acad. Sci. USA 109, 13471–13472. https://doi.org/10.1073/pnas.1211082109.

Hublin, J.-J., 2015. The modern human colonization of western Eurasia: When and where? Quat. Sci. Rev. 118, 194–210. https://doi.org/10.1016/j.quascirev.2014.08.011.

Hublin, J.-J., Spoor, F., Braun, M., Zonneveld, F.W., Condemi, S., 1996. A late Neanderthal associated with Upper Palaeolithic artefacts. Nature 381, 224–226. https://doi.org/10.1038/381224a0.

Kanazawa, E., Sekikawa, M., Ozaki, T., 1990. A quantitative investigation of irregular cuspules in human maxillary permanent molars. Am. J. Phys. Anthropol. 83, 137–274. https://doi.org/10.1002/ajpa.1330830205.

Keen, H.J., 1966. A morphologic and biometric study of taurodontism in a contemporary population. Am. J. Phys. Anthropol. 25, 208–209.

Kupczik, K., Hublin, J.-J., 2010. Mandibular molar root morphology in Neanderthals and Late Pleistocene and recent Homo sapiens. J. Hum. Evol. 59, 525–541. https://doi.org/10.1016/j.jhevol.2010.05.009.

Le Cabec, A., Gunz, P., Kupczik, K., Braga, J., Hublin, J.-J., 2013. Anterior tooth root morphology and size in Neanderthals: Taxonomic and functional implications. J. Hum. Evol. 64, 169–193. https://doi.org/10.1016/j.jhevol.2012.08.011.

Le Cabec, A., Tang, N., Tafforeau, P., 2015. Accessing developmental information of fossil hominin teeth using new synchrotron microtomography-based visualization techniques of dental surfaces and interfaces. PLoS One 10, e0123019. https://doi.org/10.1371/journal.pone.0123019.

Leroi-Gourhan, A., 1951. Informations, antiquités préhistoriques. Gallia 6, 241–247.

Leroi-Gourhan, A., 1951. Les fouilles d'Arcy-sur-Cure (Yonne). Gallia Prehist. 4, 3–16.

Leroi-Gourhan, A., 1952. Stratigraphie et découvertes récentes dans les grottes d'Arcy-sur-Cure (Yonne). Rev. Géogr. Lyon 27, 425–433. https://doi.org/10.3406/GEOCA.1952.1168.

Leroi-Gourhan, A., 1958. Étude des restes humains fossiles provenant des Grottes d'Arcy-sur-Cure. Ann. Paleontol. 44, 87–148.

Liversidge, H.M., Molleson, T., 2004. Variation in crown and root formation and eruption of human deciduous teeth. Am. J. Phys. Anthropol. 123, 172–180. https://doi.org/10.1002/ajpa.10318.

Macchiarelli, R., Bondioli, L., Debénath, A., Mazurier, A., Tournepiche, J.-F., Birch, W., Dean, C., 2006. How Neanderthal molar teeth grew. Nature 444, 748–751. https://doi.org/10.1038/nature05314.

Mafessoni, F., Grote, S., de Filippo, C., Slon, V., Kolobova, K.A., Viola, B., Markin, S.V., Chintalapati, M., Peyrégne, S., Skov, L., Skoglund, P., Krivoshapkin, A.I., Derevianko, A.P., Meyer, M., Kelso, J., Peter, B., Prüfer, K., Pääbo, P., 2020. A high-coverage neandertal genome from chagyrskaya Cave. Proc. Natl. Acad. Sci. USA 117, 15132–15136. https://doi.org/10.1073/pnas.2004944117.

Martin, R., Saller, K., 1957. Lehrbuch der Anthropologie. Gustav Fischer Verlag, Stuttgart.

Martin, R.M.G., Hublin, J.-J., Gunz, P., Skinner, M.M., 2017. The morphology of the enamel dentine junction in Neanderthal molars: Gross morphology, non-metric traits, and temporal trends. J. Hum. Evol. 103, 20–44. https://doi.org/10.1016/j.jhevol.2016.12.004.

Martínez de Pinillos, M., Martinón-Torres, M., Skinner, M.M., Arsuaga, J.L., Gracia-Téllez, A., Martínez, I., Martín-Francés, L., Bermúdez de Castro, J.M., 2014. Trigonid crests expression in Atapuerca-Sima de los Huesos lower molars: Internal and external morphological expression and evolutionary inferences. C. R. Palevol 13, 205–221. https://doi.org/10.1016/j.crpv.2013.10.008.

Martinón-Torres, M., Bermúdez de Castro, J.M., Gómez-Robles, A., Prado-Simón, L., Arsuaga, J.L., 2012. Morphological description and comparison of the dental remains from Atapuerca-Sima de los Huesos site (Spain). J. Hum. Evol. 62, 7–58. https://doi.org/10.1016/j.jhevol.2011.08.007.

Martinón-Torres, M., Martínez de Pinillos, M., Skinner, M.M., Martín-Francés, L., Gracia-Téllez, A., Martínez, I., Arsuaga, J.L., Bermúdez de Castro, J.M., 2014. Talonid crests expression at the enamel-dentine junction of hominin lower permanent and deciduous molars. C. R. Palevol 13, 223–234. https://doi.org/10.1016/j.crpv.2013.12.002.

Maureille, B., Hublin, J.-J., 2019. L'Homme châtelperronien de la Grotte du Renne et l'inventaire des vestiges humains des grottes d'Arcy-sur-Cure. In: Julien, M., David, F., Girard, M., Roblin-Jouve, A. (Eds.), Le Châtelperronien de la grotte du Renne (Arcy-sur-Cure, Yonnem, France), PALEO, Spec. num, pp. 365–408.

Maureille, B., Costamagno, S., Beauval, C., Mann, A.E., Garralda, M.D., Mussini, C., Laroulandie, V., Rendu, W., Royer, A., Seguin, G., Vandermeersch, B., 2017. The challenges of identifying partially digested human teeth: First description of Neandertal remains from the Mousterian site of Marillac (Marillac-le-Franc, Charente, France) and implications for palaeoanthropological research. Paléo 28, 201–212.

Mays, S., 2016. Bone-formers and bone-losers in an archaeological population. Am. J. Phys. Anthropol. 159, 577–584. https://doi.org/10.1002/ajpa.22912.

Miles, A.E.W., 2001. The Miles method of assessing age from tooth wear revisited. J. Archaeol. Sci. 28, 973–982. https://doi.org/10.1006/jasc.2000.0652.

Molnar, S., 1971. Human tooth wear, tooth function and cultural variability. Am. J. Phys. Anthropol. 34, 175–189. https://doi.org/10.1002/ajpa.1330340204.

Moorrees, C.F.A., Fanning, E.A., Hunt, E.E., 1963. Age variation of formation stages for ten permanent teeth. J. Dent. Res. 42, 1490–1502. https://doi.org/10.1177/00220345630420062701.

Mussini, C., 2011. Les restes humains moustériens des Pradelles (Marillac-le-Franc, Charente, France) : étude morphométrique et réflexions sur un aspect comportemental des Néandertaliens. Université de Bordeaux 1, Bordeaux, 478 p.

Pederzani, S., Britton, K., Trost, M., Fewlass, H., Bourgon, N., McCormack, J., Jaouen, K., Dietl, H., Döhle, H.-J., Kirchner, A., Lauer, T., Le Corre, M., McPherron, S.P., Meller, H., Mylopotamitaki, D., Orschiedt, J., Rougier, H., Ruebens, K., Schüler, T., Sinet-Mathiot, V., Smith, G.M., Talamo, S., Tütken, T., Welker, F., Zavala, E.I., Weiss, M., Hublin, J.-J., 2024. Stable isotopes show *Homo sapiens* dispersed into cold steppes ~45,000 years ago at Ilsenhöhle in Ranis, Germany. Nat. Ecol. Evol. 8, 578–588. https://doi.org/10.1038/s41559-023-02318-z.

Peyrégne, S., Slon, V., Mafessoni, F., de Filippo, C., Hajdinjak, M., Nagel, S., Nickel, B., Essel, E., le Cabec, A., Wehrberger, K., Cnard, N.J., Kind, C.J., Posth, C., Krause, J., Abrams, G., Bonjean, D., di Modica, K., Toussaint, M., Kelso, J., Meyer, M., Pääbo, S., Prüfer, K., 2019. Nuclear DNA from two early Neandertals reveals 80,000 years of genetic continuity in Europe. Sci. Adv. 5, eaaw5873. https://doi.org/10.1126/sciadv.aaw5873.

Ramirez Rozzi, F., Bermudez de Castro, J., 2004. Surprisingly rapid growth in Neanderthals. Nature 428, 936–939. https://doi.org/10.1038/nature02428.

Roblin-Jouve, A., Miskowsky, J.-C., Hardy, M., Girard, M., David, F., 2018. Étude stratigraphique, lithologique et sédimentologique de la Grotte du Bison à Arcy-sur-Cure (Yonne). L'Anthropologie 122, 589–609. https://doi.org/10.1016/j.anthro.2018.09.003.

Roksandic, M., Armstrong, S.D., 2011. Using the life history model to set the stage(s) of growth and senescence in bioarchaeology and paleodemography. Am. J. Phys. Anthropol. 145, 337–347. https://doi.org/10.1002/ajpa.21508.

Scott, G.R., Irish, J.D., 2017. Human Tooth Crown and Root Morphology. Cambridge University Press, Cambridge. https://doi.org/10.1017/9781316156629.

Sempé, M., 1978. Auxologie: Méthode et Séquences. Laboratoire Théraplix, Paris.

Shackelford, L.L., Stinespring Harris, A.E., Konigsberg, L.W., 2012. Estimating the distribution of probable age-at-death from dental remains of immature human fossils. Am. J. Phys. Anthropol. 147, 227–253. https://doi.org/10.1002/ajpa.21639.

Skinner, M.M., Gunz, P., 2010. The presence of accessory cusps in chimpanzee lower molars is consistent with a patterning cascade model of development. J. Anat. 217, 245–253. https://doi.org/10.1111/j.1469-7580.2010.01265.x.

Skinner, M.M., Wood, B.A., Boesch, C., Olejniczak, A.J., Rosas, A., Smith, T.M., Hublin, J.-J., 2008. Dental trait expression at the enamel-dentine junction of lower molars in extant and fossil hominoids. J. Hum. Evol. 54, 173–186. https://doi.org/10.1016/j.jhevol.2007.09.012.

Slimak, L., Zanolli, C., Higham, T., Frouin, M., Schwenninger, J.-L., Arnold, L.J., Demuro, M., Douka, K., Mercier, N., Guérin, G., Valladas, H., Yvorra, P., Giraud, Y., Seguin-Orlando, A., Orlando, L., Lewis, J.E., Muth, X., Camus, H., Vandevelde, S., Buckley, M., Mallol, C., Stringer, C., Metz, L., 2022. Modern human incursion into Neanderthal territories 54,000 years ago at Mandrin, France. Sci. Adv. 8, eabj9496. https://doi.org/10.1126/sciadv.abj9496.

Slimak, L., Vimala, T., Seguin-Orlando, A., Metz, L., Zanolli, C., Joannes-Boyau, R., Frouin, M., Arnold, L.J., Demuro, M., Devièse, T., Comeskey, D., Buckley, M., Camus, H., Muth, X., Lewis, J.E., Bocherens, H., Yvorra, P., Tenailleau, C., Duployer, B., Coqueugniot, H., Dutour, O., Higham, T., Sikora, M., 2024. Long genetic and social isolation in Neanderthals before their extinction. Cell Genom 4, 100593. https://doi.org/10.1016/j.xgen.2024.100593.

Smith, B.H., 1984. Patterns of molar wear in hunter-gatherers and agriculturists. Am. J. Phys. Anthropol. 63, 39–56.

Smith, T.M., Toussaint, M., Reid, D.J., Hublin, J.-J., 2007. Rapid dental development in a middle paleolithic Belgian neanderthal. Proc. Natl. Acad. Sci. USA 104, 20220–20225. https://doi.org/10.1073/pnas.0707051104.

Smith, T.M., Tafforeau, P., Reid, D.J., Pouech, J., Lazzari, V., Zermeno, J.P., Guatelli-Steinberg, D., Olejniczak, A.J., Hoffman, A., Radovčić, J., Makaremi, M., Toussaint, M., Stringer, C., Hublin, J.-J., 2010. Dental evidence for ontogenetic differences between modern humans and Neanderthals. Proc. Natl. Acad. Sci. USA 107, 20923–20928. https://doi.org/10.1073/pnas.1010906107.

Tillier, A.-M., Sansilbano-Collilieux, M., David, F., Enloe, J.G., Girard, M., Hardy, M., D'Iatchenko, V., Roblin-Jouve, A., Tolmie, C., 2013a. Les vestiges néandertaliens provenant des niveaux moustériens I et J de la grotte du Bison à Arcy-sur-Cure (Yonne): Bilan actuel. Bull. Mem. Soc. Anthropol. Paris 25, 39–54. https://doi.org/10.1007/s13219-012-0061-7.

Tillier, A.-M., Hardy, M., David, F., Girard, M., D'Iatchenko, V., 2013b. À propos de deux molaires déciduales inférieures provenant des niveaux moustériens de la grotte du Bison (Arcy-sur-Cure, Yonne, France). Paléo 24, 271–278. https://doi.org/10.4000/paleo.2685.

Welker, F., Hajdinjak, M., Talamo, S., Jaouen, K., Dannemann, M., David, F., Julien, M., Meyer, M., Kelso, J., Barnes, I., Brace, S., Kamminga, P., Fischer, R., Kessler, B.M., Stewart, J.R., Pääbo, S., Collins, M.J., Hublin, J.-J., 2016. Palaeoproteomic evidence identifies archaic hominins associated with the Châtelperronian at the Grotte du Renne. Proc. Natl. Acad. Sci. USA 113, 11162–11167. https://doi.org/10.1073/pnas.1605834113.

White, T.D., Folkens, P.A., 2005. The Human Bone Manual. Academic Press, San Diego.

Wickham, H., 2016. ggplot2: Elegant Graphics for Data Analysis. Springer, New York. https://ggplot2.tidyverse.org/.